Search for Charged Higgs Bosons at LEP200 using the DELPHI Detector

Cand. Scient. Thesis in Experimental Particle Physics

Yngve Kvinnsland

Department of Physics
University of Oslo

October 10, 1996

Abstract

An analysis has been designed to find Charged Higgs events with the DELPHI detector at LEP200 assuming $B(H^{\pm} \to \tau\nu_{\tau}) = 1$.

Simulations show that if most of the runs are done with $\sqrt{s} = 192$ and 300 pb^{-1} is collected as planned, the present mass limit can be lifted about 30 GeV to 75 GeV. Discovery is possible if the mass is lower than 58 GeV.

The best energy to look for a Charged Higgs is just below W-pair threshold at $\sqrt{s} \approx 160$ GeV. At higher energies the irreducible background from W-pairs is comparable to the signal.

During the autumn 1995 5.9 pb^{-1} were collected with the DELPHI detector at $\sqrt{s} = 130 - 136$ GeV. These data, the P3-data, are analyzed and zero Charged Higgs candidates are found. This result does not improve the present mass limit.

Acknowledgements

I thank my supervisor, Alex Read, first of all for giving me the idea of doing this interesting and challenging work, but also for his support and inspiration on the way. A special thank goes to Trond Myklebust for always helping me out with my numerous computer problems and for being very patient with me. I would also like to thank my fellow students, Esben and Vidar Lund, Bernt Olav Rostad, Håkon Fløystad, Anne-Kari Ytrestøl, Harald Meland, and Jørgen Hansen (with whom I have shared an office and who has cheered me up with lively whistling and everlasting enthusiasm) for interesting discussions and a good atmosphere.

Contents

1 Introduction

In 1932 physicists knew of four elementary particles, the proton, the neutron, the electron and the photon. Twenty years later the number was fifteen and during the fifties it continued to grow. The situation resembled the one in the 19th century when most of the chemical elements were discovered. There was a need for a systematic classification, something like Mendeleevs periodic table.

In 1960-61 Murray Gell-Mann and Yuval Ne'eman independently discovered that the particles could be assigned to *multiplets* with eight and ten members. Gell-Mann saw that in one of these multiplets there was an empty space and predicted the existence of Ω^-, a particle with spin $\frac{3}{2}$ and certain decay channels. It was discovered in 1964 with the correct properties.

The underlying structure of this classification scheme is the structure of the symmetry group $SU(3)$[1]. By studying decays it could be deduced in which multiplets the particles belong. There is a close connection between the branching ratios and the Clebsch-Gordan coefficients, the numbers describing the relation between the various multiplets.

What Gell-Mann and Ne'eman had done was to find the *symmetry* of the system. When the symmetry was discovered predictions could be made about which decays were legal and which were not. Also, when there was an incomplete multiplet one knew that there were particles yet to be discovered. Finding the symmetry has become the ultimate question in particle physics.

Today, the particles considered as elementary are the quarks and the leptons. All the particles discovered in the fifties and sixties are formed by two or three quarks. In addition there are gauge bosons which mediate the forces relevant when looking at the microscopic world, that is the electromagnetic, the weak and the strong force.

For several reasons it is widely believed that the interactions are described by a *gauge* theory[2, 3], a theory *defined* by a symmetry. The basic idea behind this theory is that the interactions are invariant under certain gauge transformations. However, this assumption leads to the problematic prediction that all particles have zero mass, and this is indeed not in agreement with experiments or everyday experiences. Another problem is that at high energies certain processes have a probability above one.

The *Higgs mechanism* invented by Peter W. Higgs gives a solution to both these problems. In a very elegant and simple manner it gives masses to the particles and no processes have probabilities above one. Following the introduction of a Higgs field comes the prediction of Higgs bosons.

It is not given what the Higgs field should look like. Various choices give different numbers of Higgs particles. Except for the simplest choice with one

doublet there will be charged Higgs bosons, $H^{\pm}$. The subject of this thesis is how to search for these particles using the DELPHI detector at LEP200. More specifically it is a search for charged Higgs particles decaying only to taus and tau-neutrinos.

LEP is the Large Electron Positron accelerator situated at CERN, the European Laboratory for Particle Physics, in a 27 km long tunnel. It was built during the 80's mainly to produce Z^0's, and with an energy of 91 GeV it is the worlds largest electron-positron collider. The tunnel houses four independent experiments: DELPHI, OPAL, L3 and ALEPH. Norwegian physicists are members of the DELPHI Collaboration.

As this is written an upgrading of LEP is in progress, one is going from LEP1 to LEP2. The energy is increased up to 192 GeV with intermediate running at 130-136 GeV, 161 GeV and 175 GeV. The runs at 130-136 and 161 GeV are completed but only the 130-136 GeV data are available for analysis.

According to the Particle Data Group[4] the highest 95% confidence mass limit obtained so far is the limit published in [5] by the DELPHI Collaboration. For a charged Higgs with $B(H^{\pm} \to \tau\nu_{\tau}) = 1$ it is 45.4 GeV, with no assumptions about the decay it is 43.5 GeV. The second and the third best limits are obtained by two of the other LEP experiments, L3 and ALEPH. L3 has excluded masses up to 44 GeV with $B(H^{\pm} \to \tau\nu_{\tau}) > 0.4$ and up to 41 GeV for arbitrary $B(H^{\pm} \to \tau\nu_{\tau})$[6]. ALEPH has for $B(H^{\pm} \to \tau\nu_{\tau}) = 1$ a limit of 45.3 GeV and for arbitrary $B(H^{\pm} \to \tau\nu_{\tau})$ 41.7 GeV[7].

The first sections in this thesis are intended to give some understanding of the Higgs mechanism, they give the motivation for doing Higgs searches. Then a brief discussion of the DELPHI detector is given so that one can get a feeling for the process of event reconstruction.

After these opening sections the analysis can be presented. The intention is not only to give a description of the analysis but also to give some understanding of the ideas behind it. The subsequent examination of the results from simulations is also meant to illustrate how the analysis works. Finally the data accumulated at 130-136 GeV (also called the 95-P3 data) are treated.

2 The Higgs Mechanism

It is an amazing fact that the couplings of the Standard Model can be derived only by demanding what is called local gauge invariance. As an example of gauge invariance one can study the electromagnetic interactions.

In the absence of external forces fermions obey the relativistic Dirac equation

$$(i\gamma^\mu \partial_\mu - m)\psi(x) = 0. \tag{1}$$

Demanding local U(1) invariance means that the transformation

$$\psi(x) \to \psi'(x) = e^{-iqf(x)}\psi(x) \tag{2}$$

should leave (1) invariant where f is an arbitrary function. It is quite obvious that this is not the case unless something more than transforming the field is done. The solution is to substitute the derivatives:

$$\partial_\mu \to D_\mu = [\partial_\mu + iqA_\mu(x)] \tag{3}$$

and let the gauge field A transform as

$$A_\mu(x) \to A'_\mu(x) = A_\mu(x) + \partial_\mu f(x). \tag{4}$$

(1) becomes

$$(i\gamma^\mu \partial_\mu - m)\psi(x) = -e\gamma^\mu A_\mu \psi(x). \tag{5}$$

The coupled transformation (2) and (4) is referred to as a gauge transformation and (5) is gauge invariant. If $q = -e$ and A is interpreted as the electromagnetic potential this is nothing else but the equation for the electron in an electromagnetic field which is the basis for QED (quantum electro dynamics). Technically speaking q is the generator of a $U(1)$ symmetry group of electromagnetic interactions.

Electromagnetism and weak interactions are unified in what is called the *electroweak* theory[8]. This theory is invariant under $SU(2)_L \times U(1)_Y$ transformations. $SU(2)_L$ invariance means invariance under rotations in the weak isospin space while $U(1)_Y$ invariance means that phase transformations like (2) with the hypercharge, Y, as the generator, should leave the physics unaltered. If one starts with (1) and demands that the physics should be invariant under $SU(2)_L \times U(1)_Y$ the electroweak theory emerges just as QED did. If in addition invariance under rotations in colour space is imposed, the strong interactions are added to the theory.

The problem arising when requiring gauge symmetry in the electroweak sector, is that masses are forbidden as they break the symmetry. In other

words, no particles can have masses. This is not at all in agreement with what we see.

So, why don't we discard the symmetry and allow the masses? One reason for not doing this is that gauge invariant theories are renormalizable[9], i.e. infinities appearing when higher order terms are included can be removed in a systematic way.

Symmetries are best discussed in the framework of Lagrangian field theory[10]. Different terms in a Lagrangian are interpreted as interactions, kinetic energies, potential energies and finally mass terms. In a gauge theory mass terms like $\frac{1}{2}mA_\mu A^\mu$ are forbidden because they break the symmetry. Given the Lagrangian, $\mathcal{L}$, as a function of the fields $\phi_r(x)$ the field equations are derived by substituting for $\mathcal{L}$ in the Euler-Lagrange equations

$$\frac{\partial \mathcal{L}}{\partial \phi_r} - \frac{\partial}{\partial x^\mu}\left(\frac{\partial \mathcal{L}}{\partial \phi_{r,\mu}}\right) = 0 \tag{6}$$

where $\phi_{r,\mu} \equiv \frac{\partial \phi_r}{\partial x^\mu}$.

Before entering the mathematics of the Higgs Mechanism it is appropriate with an analogy. Consider an infinitely extended ferromagnet. The equations describing this system are invariant under rotations. In the ground state all the elementary spins are aligned in a particular direction. This direction is arbitrary and the system does not have a rotational symmetry.

The point is that one particular state is not invariant under rotational symmetry while the equations describing the system are. This is what is going on in the Higgs mechanism. A new field possessing the $SU(2)_L \times U(1)_Y$ symmetry is added. Then a particular ground state is chosen and the symmetry is thereby broken. This is called spontaneous symmetry breaking.

As the mathematics of local $SU(2)_L \times U(1)_Y$ symmetry breaking is rather complicated a much simpler example will be used to illuminate the process, the spontaneous breaking of a $U(1)$ symmetry. Consider the Lagrangian of a complex scalar field $\phi = (\phi_1 + i\phi_2)/\sqrt{2}$:

$$\mathcal{L} = (\partial_\mu \phi)^*(\partial^\mu \phi) - \mu^2 \phi^* \phi - \lambda(\phi^* \phi)^2 \tag{7}$$

As shown above we now demand this Lagrangian to be invariant under $U(1)$ transformations so that the result is a $U(1)$ gauge invariant Lagrangian:

$$\mathcal{L} = (\partial^\mu + ieA^\mu)\phi^*(\partial_\mu - ieA_\mu)\phi - \mu^2 \phi^* \phi - \lambda(\phi^* \phi)^2 - \frac{1}{4}F_{\nu\mu}F^{\mu\nu} \tag{8}$$

where $F_{\mu\nu} \equiv \partial_\mu A_\nu - \partial_\nu A_\mu$. The last term, a kinetic energy term, is not necessary to restore the symmetry, but if we look at A as a physical field, the kinetic energy should be added, and it does not break the symmetry.

The potential of (7) is $V(\phi) = \mu^2\phi^*\phi + \lambda(\phi^*\phi)^2$. Now assume that $\lambda > 0$ and $\mu^2 < 0$. Then there is a circle of minima in the ϕ_1, ϕ_2 plane with radius v where

$$v^2 = -\frac{\mu^2}{\lambda}. \tag{9}$$

$\phi = 0$ does not represent an energy minimum. It is natural to write the potential as fluctuations around a minimum, so a change of variables is done. However, as there is a circle of minima a particular choice of ground state has to be chosen. This is the symmetry breaking. As there is no preferred choice of direction one might as well use $\phi_1 = v$ and $\phi_2 = 0$. The field can now be written as

$$\phi(x) = \sqrt{\frac{1}{2}}(v + h(x))e^{i\theta(x)/v} \tag{10}$$

ϕ can be thought of as a vector in the complex plane with length $v + h$. The angle between the real axis and the vector is θ/v. As the potential is invariant under rotations the physics should be independent of θ, and this is indeed the case.

The thing now is that there is no difference between giving $\theta(x)$ a certain value in (10) and doing the transformation (2) with $f(x) = \theta(x)$. That is, one of the degrees of freedom corresponds to the freedom to make a gauge transformation. When this is discovered the gauge field must undergo the appropriate transformation, that is the transformation corresponding to the transformation $\phi \to e^{i\theta(x)/v}\phi$:

$$A_\mu \to A_\mu + \frac{1}{ev}\partial_\mu\theta \tag{11}$$

The resulting Lagrangian is

$$\mathcal{L} = \frac{1}{2}(\partial_\mu h)^2 - \lambda v^2 h^2 + \frac{1}{2}e^2v^2A_\mu^2 - \lambda v h^3 - \frac{1}{4}\lambda h^4 + \frac{1}{2}e^2A_\mu^2h^2 + ve^2A_\mu^2h - \frac{1}{4}F_{\mu\nu}F^{\nu\mu}. \tag{12}$$

Here we have a massive scalar h with $m = \sqrt{2\lambda v^2}$ and most important, the gauge field has acquired a mass $m = ev$.

The spontaneous breaking of the $SU(2) \times U(1)$ invariance is done in the same way, except that a Higgs doublet or more complicated Higgs representations has to be used instead of a singlet. Fermions are given masses by adding a coupling term between the Higgs doublets and the fermion fields.

It is not obvious that the Standard Model is renormalizable with this spontaneously broken symmetry. The proof by 't Hooft was not completed before 1971.

3 The Charged Higgs

When the $SU(2)_L \times U(1)_Y$ symmetry in the electroweak sector of the Standard Model is broken with one Higgs doublet, one neutral Higgs particle is introduced. So, where is the charged Higgs?

Only one doublet is *needed* to break $SU(2)_L \times U(1)_Y$. However, there is no reason not to introduce a more complicated Higgs sector. This will result in phenomena like the charged Higgs.

There are a few theoretical arguments that place some general constraints on the Higgs sector. First, it is an experimental fact that $\rho = M_W^2/(M_Z^2 \cos^2 \theta_w)$ is very close to one. In the standard model this value is determined by the Higgs sector, and with one doublet $\rho = 1$ automatically. However, this is also true for any number of singlets and doublets[11].

The second constraint is the severe limits on flavour-changing neutral currents (FCNC). A theorem of Glashow and Weinberg[12] states that in a model with more than one doublet FCNC's are absent if all fermions of a particular charge couple to only one doublet.

A third requirement of the Higgs sector is that high-energy divergences of processes like $W^+W^- \to W^+W^-$ must be canceled out.

In this thesis the charged Higgs of a model with two doublets will be considered. Attractive features of a two-doublet model are:

- The low number of parameters.
- ρ is automatically equal to one.
- It is easy to choose couplings so that FCNC's are absent.
- The high-energy divergences in the Standard Model are canceled out.

In the previous section U(1) symmetry was broken by the help of a Higgs singlet. As the singlet is complex it contains two degrees of freedom. Gauge invariance was established by introducing one gauge field. As was shown, one of the degrees of freedom corresponded to the freedom to make a gauge transformation, and did not result in any particle. In the Standard Model, when breaking the symmetry in the electroweak theory, a doublet with four degrees of freedom is used. Four gauge fields are needed for $SU(2)_L \times U(1)_Y$ gauge symmetry. However, U(1) symmetry is retained for the electromagnetic interactions ($U(1)_{em}$ is a subset of $SU(2)_L \times U(1)_Y$) leaving the photon massless. Only three of the degrees of freedom are absorbed by the gauge fields, and one Higgs particle emerges.

Using two Higgs doublets instead of one gives four extra degrees of freedom, the total is five. This gives a much richer particle content. Three

neutrals, A^0, H^0 and h^0, and finally two charged Higgs particles, $H^\pm$, with equal mass.

As the charged Higgs bosons have equal mass, there must be another degree of freedom in addition to the masses. This is the ratio between the vacuum expectation values of the two Higgs doublets, usually denoted by $\tan\beta$.

In order to remove FCNC's it suffices to make all fermions with a particular charge couple to one doublet only. However there are still several choices of couplings to the fermions. One possibility is to let all the fermions couple to only one of the Higgs doublets. This is what is denoted as Model I in [13]. Another choice is to let ϕ_1 couple to down-type quarks and leptons and ϕ_2 to up-type quarks and neutrinos. This is denoted as Model II.

The expression for $\sigma_{H^\pm}$ used in this thesis is independent of which of the two models is used. The coupling between Higgs particles and gauge bosons are the same. What is model dependent are the couplings to fermions.

As an example, consider the term in the Lagrangian describing the interaction between charged Higgs bosons and fermions. In Model I it is given by

$$\frac{g\cot\beta}{2\sqrt{2}M_W}(H^+\bar{U}[M_U K(1-\gamma_5) - K M_D(1+\gamma_5)]D + h.c.)$$

and in Model II by

$$\frac{g}{2\sqrt{2}M_W}(H^+\bar{U}[\cot\beta M_U K(1-\gamma) + \tan\beta K M_D(1+\gamma_5)]D + h.c.).$$

where h.c. means hermitian conjugate terms. K is the CKM mixing matrix (Cabibbo-Kobayashi-Maskawa), M_D and M_U are diagonal mass matrixes for respectively down-type quarks (leptons) and up-type quarks (neutrinos). $K = 1$ for leptons. One can see that the couplings are proportional to the masses which is typical for all Higgs couplings. In Model I $\tan\beta$ is determining the strength of the coupling to fermions and the $\tan\beta$ dependence is the same for all the couplings. In Model II the dependence is related to the masses. For the coupling between a charged Higgs and a pair of fermions, large $\tan\beta$ favours heavy down-type quarks (leptons), small $\tan\beta$ favours heavy up-type quarks (neutrinos).

This means that by giving $\tan\beta$ a value that is large enough the branching ratio of the charged Higgs to the heaviest kinematically allowed lepton and the corresponding neutrino will be larger than the branching ratio to any quark pair given that the heaviest allowed down-type quark is lighter than the lepton. Even though the b-quark is more than twice as heavy as the τ-lepton, as long as the t-quark is not allowed large $\tan\beta$ will give large branching ratios to $\tau\nu_\tau$. The reason is that the bc decay is suppressed by

the CKM matrix. Small $\tan\beta$ will give large branching ratios to cs. This thesis is treating charged Higgs particles with $B(H \to \tau\nu) = 1$ and as this discussion has shown this is equivalent to large $\tan\beta$ in Model II.

A theory given much attention in recent years and which some have considered as promising, is Supersymmetry[13]. The minimal version, The Minimal Supersymmetric Extension of the Standard Model (MSSM), contains two Higgs doublets and the Higgs-fermion couplings are those of Model II. The cross section for charged Higgs production in an e^+e^- collider is the same as the one derived in appendix A.

In a supersymmetric model the number of free parameters in the Higgs sector is lower due to the additional symmetry. Without supersymmetry there were five parameters, the Higgs masses and $\tan\beta$. In the MSSM model there are two. Usually $\tan\beta$ and $M_{H^\pm}$ are adopted as the independent parameters. The other masses are functions of these.

Specifically the mass of A^0 is related to $M_{H^\pm}$ by

$$M_{A^0}^2 = M_{H^\pm}^2 - M_W^2.$$

This means that the mass of the charged Higgs must be greater than the mass of the W. As A^0 has been excluded up to masses of 22 GeV, the limit is even higher. A discovery of a charged Higgs with a mass below 83 GeV therefore eliminates MSSM as a possible theory.

As an experimentalist one should not be overly concerned with which theory one is trying to confirm or reject. This search should be looked at simply as a search for a charged scalar with $B(H^\pm \to \tau\nu) = 1$, not as a search for the charged Higgs of a Model II of a two-doublet Higgs Sector. If a charged scalar is found, it could as an example equally well be a technipion[14]. One can never know for sure what the theory should be like, but the inspiration for doing this search comes from the Higgs models containing charged Higgs bosons.

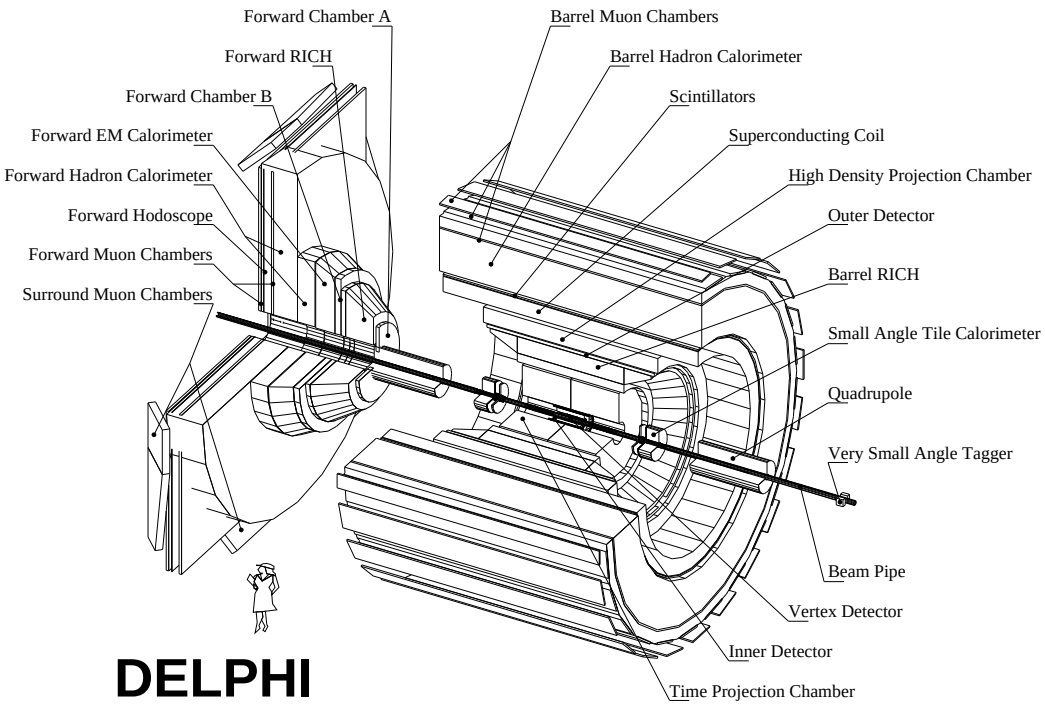

Figure 1: The Delphi Detector.

4 The DELPHI Detector

DELPHI[15], a DEtector with Lepton, Photon and Hadron identification, is one out of four detectors operating at LEP. It is a 4π detector designed with emphasis on particle identification, but at the same time it is a general purpose detector.

The detector is installed in a cavern 100 m below ground. It can be divided in two parts, the cylindrical barrel and the endcaps. See figure 1 for an overview of the whole detector. The endcaps can be moved parallelwise to the beam pipe giving easy access to the detector.

The barrel covers the polar region from 45° to 135° while the endcaps cover the regions $10^\circ - 40^\circ$ and $140^\circ - 170^\circ$. In the intermediate regions the detection is incomplete and this represents a weakness of the DELPHI detector. New subdetectors have been installed to improve on this, but detection in this polar region is still a problem. For a description of the performance of the DELPHI detector, see [16].

In the descriptions given below, terms like "drift chamber", "Multi Wire Proportional Chamber" or "Silicon Strip Detector" will not be explained. See [17] for an introduction to the various detector types.

	R [cm]	$\|z\|$ [cm]	θ [deg]
Vertex Det.	6.3/9.0/11.3	12	11-169
ID: jet	11.8-22.3	≤ 105	15-165
ID: trigger	23-28	≤ 105	15-165
TPC	35-111	≤ 134	20-160
OD	198-206	≤ 232	43-137
B-Muon	~ 445	≤ 185	52-138
	~ 485		
F-CHA	30-103	155-165	11-33
F-CHB	53-195	267-283	11-35
F-Muon	70-460	463	9-43
		500	

Table 1: Regions covered by the tracking detectors.

4.1 The Superconducting Solenoid

Determination of charged particles momenta in the DELPHI detector is based on measurements of the curvature of the particle trajectories which is a result of the magnetic field produced with the solenoid. The solenoid has a length of 7.4 m and an inner diameter of 5.2 m. The current of 5000 A sets up a magnetic field in the beam direction of 1.2 T. The azimuthal variation is negligible and the radial component is < 5 G, requirements necessary for good track reconstruction. The solenoid is cooled by liquid helium at 4.5 K.

4.2 Tracking Detectors

This section gives a brief description of the tracking detectors, that is the detectors used for track reconstruction. Table 1 gives an overview of the regions covered.

Vertex Detector The main purpose of this detector is to provide maximum $R\phi$-resolution, in particular for the study of heavy flavour physics. It consists of three concentric shells of Si-strip detectors at radii of 6.3 (Closer), 9.0 (Inner) and 11.0 (Outer layer) cm which cover the central region over a length of 24.0 cm. Each shell consists of 24 modules with four detectors along z. The resolution is $5\mu m$ for single tracks and the double track separation is less than $100\mu m$.

In order to increase the angular angle acceptance endcaps are added to the VD before LEP200 runs[18]. They are called the Very Forward

Tracker (VFT). Motivations for doing this are that the channels with the largest cross sections ($f\bar{f}\gamma$, $\gamma\gamma$ channels) are peaked in the forward direction and Higgs searches require good hermeticity. The VFT cover the polar angles $11^\circ - 25^\circ$ and $155^\circ - 169^\circ$.

The space point resolution is expected to be better than $70\mu m$ and the angular resolution better than 1 mrad.

Inner Detector The ID is made up of two concentric parts, an inner drift chamber and 5 straw tube detector layers. The straw detector was installed in 1995 substituting MWPC's[19, 20].

The drift chamber has jet-chamber geometry with 24 points in $R - \phi$. It is divided into 24 azimuthal sectors. It has a single wire precision of 85 μm and local track element precisions of $\sigma(R\phi) = 40$ μm and $\sigma(\phi) = 0.89$ mrad.

The straw detector has a length of 2.1 m and consist of 5 concentric layers. Each layer has 192 straw tubes. It provides $R\phi$ measurements used in triggering and for solving left/right ambiguities in the jet-chamber.

Time Projection Chamber The TPC is the principal tracking device of the DELPHI detector. It extends radially from 35 to 111 cm and to $|z| = 134$ cm in z giving a polar acceptance of 20° to 160°.

At $z = 0$ there is a high voltage plane dividing it into two drift chambers. At the endcaps there are MWPC's consisting of 6 sector plates with 192 wires. The drift velocity is 66.94 ± 0.07 mm/μs and the number of ionized electrons is about 70 per cm of gas. The MWPC's can provide up to 16 space points for a non-looping particle.

The $R\phi$ resolution is in the range 180-280 μm (depending on ϕ and z), in z it is about 900 μm. The TPC also provides a measurement of dE/dx with a resolution of $\sigma = 5.8\%$ for muons at 45 GeV and 7.5% for pions between 280 and 400 MeV.

Outer Detector The OD was introduced in order to improve the momentum resolution in $R\phi$. It also gives some trigger information.

It is composed of 24 modules, each covering a 15° sector in ϕ. Every module contains 145 drift tubes in 5 layers. The OD is shaped as a cylinder with radii of 198 and 206 cm and length 464 cm giving a polar acceptance of 43° to 137°. The structure provides 5 space points in $R\phi$ and 3 in z.

The resolutions are 300 μm in $R\phi$ and 4.4 cm in z.

The Muon Chambers In DELPHI there are three muon chambers, The Barrel Muon Chambers (MUB), The Surround Muon Chambers (SMC)[21] and the Forward Muon Chambers (MUF). They constitute the outer layer of the DELPHI detector.

The purpose of these detectors is to detect muons and to know that they really *are* muons. They exploit the fact that muons have the unique ability of penetrating the iron of HCAL, they are the only particles reaching these detectors.

The MUB, SMC and MUF cover a polar angle of $52° - 128°$, $40° - 50°$ $(130° - 140°)$ and $10° - 43°$ $(130° - 140°)$, respectively. The SMC were installed in 1994 to close the gap between the MUB and MUF. All the muon chambers are drift chambers.

The accuracy for the MUB is 1mm in $R\phi$ and 10mm in z. In the MUF the coordinates of a hit are determined with an uncertainty of 5mm, in the SMC with an uncertainty of 1cm.

Forward Chamber A (FCA) and Forward Chamber B (FCB) These detectors provide powerful tracking in the forward region. They are both streamer chambers. Their space resolution is about 150 μm.

4.3 Calorimetry

In DELPHI there are three types of calorimeters, the electromagnetic calorimeters, the hadronic calorimetry and the electromagnetic calorimeters for Bhabha events in the forward region. The last category is used for luminosity measurements. Table 2 shows the acceptance of the calorimeters.

When the luminosity is to be determined the defining equation $N = \sigma \cdot \mathcal{L}$ is used. N is the number of events, σ is the cross section and finally $\mathcal{L}$ is the luminosity. As the cross section for Bhabha scattering is calculable from theory this channel is well suited for luminosity measurements. In addition the cross section is very large in the forward direction, and the luminosity can therefore be determined with small uncertainties.

High Density Projection Chamber (HPC) The purpose of the HPC is to measure the three-dimensional charged distribution induced by electromagnetic showers with high granularity in all coordinates. This allows detection of e.m. showers and thereby separation from hadrons. As one of the first the HPC utilizes the time-projection principle for calorimetry.

	R [cm]	$\|z\|$ [cm]	θ [deg]
HPC	208-260	≤ 254	43-137
FEMC	46-240	284-340	10-36.5
STIC	6.5-42	220	29-185 mrad
VSAT	$\sim 6-9(\|x\|)$	770	5-7 mrad
HCAL B.	320-479	< 380	10-170
HCAL F.	65-460	340-489	

Table 2: Regions covered by the calorimeters.

In the HPC there are 41 walls spaced by 8mm gas gaps. Each wall is formed by thin lead wires glued to both sides of a fiberglass-epoxy support. A voltage gradient between neighbouring wires sets up a drift field. At one end of each module there is a single proportional wire plane reading out the ionization charge.

The HPC detector covers the barrel area inside the magnetic field with 144 separate modules using a segmentation of 24 in azimuth and 6 along z. The polar angle coverage is 43° to 137°

Forward Electromagnetic Calorimeter (FEMC) The FEMC consists of two 5 m diameter disks with a total of 9064 glass blocks. They cover polar angles $10° - 36.5°$ and $143.5° - 170°$. The lead glass counters are read out with vacuum photo triodes.

The energy resolution for Bhabha events was 4.8% in the 1994 data.

Hadron Calorimeter (HCAL) The barrel part of HCAL covers polar angles between $42.6° - 137.4°$, the endcaps $11.2° - 48.5°$ and $131.5° - 168.8°$. The barrel consists of 24 sectors with 20 layers of detectors. For each layer there are 5 cm iron plates making muons the only particles passing HCAL. The endcaps contain 19 layers constructed in a similar manner. The detectors are wire chambers which consist of a plastic cathode froming 8 cells of 9×9 mm^2 with one anode wire in each.

Performance studies on Z^0 events show that there is a good linearity between the energy measured in HCAL and the momentum obtained from the TPC for particles with energy up to 10 GeV. The resolution in HCAL is determined to $120\%/\sqrt{E}$.

Small Angle Tile Calorimeter (STIC) The STIC[22, 23] provides calorimetric coverage in the very forward direction. It was installed in 1993

replacing the SAT, the Small Angle Tagger. This was done because of the need for more accurate luminosity measurements, and the physics at LEP2 sets up new requirements. To be more precise, there was a gap in the polar coverage between the FEMC and the SAT. With the STIC installed there is no gap, and it also covers smaller polar angles than the SAT did.

The STIC is a lead-scintillator calorimeter where the light produced by the electromagnetic showers in the scintillators is carried to the photo detectors at the back of the calorimeter by means of plastic fibers. It is formed as two cylinders placed at $|z| = 220$ cm covering the angular region 29-185 mrad. It extends from 6.5 to 42 cm in radius.

Originally there was a tungsten mask in front of the STIC so that the acceptance could be determined very accurately. It has been removed in 1996 before the upgrading of LEP to LEP1.5.

Very Small Angle Tagger (VSAT) VSAT is used for fast monitoring of both luminosity and machine operation. The arms are placed at $|z| =$ 7.7 m and cover polar angles 5-7 mrad. They consist of 12 wolfram plates interleaved with silicon detectors. In addition there are three silicon planes inserted after 5,7 and 9 radiation lengths.

4.4 The DELPHI Ring Imaging Cherenkov Counter (RICH)

This detector was installed into DELPHI in order to provide particle identification. There is a barrel RICH and a forward RICH. It relies on the Cherenkov effect: particles going through matter with velocity higher than the speed of light (the speed of light in the medium in which the particle goes) radiate photons.

In both the barrel and the forward RICH there are two media, gas and liquid. The threshold Lorentz factors of the media in the barrel are $\gamma = 15.9$ and $\gamma = 1.6$, in the endcaps $\gamma = 18.3$ and $\gamma = 1.6$. The inner layer is the liquid radiators, then there is a drift tube and as the outer layer one has the gas radiators. The photons from the gas radiators are reflected back towards the drift tube with the aid of mirrors.

The angle between the direction of the radiated photons and the direction of the particle is a function of the particles speed. When the momentum is measured in the tracking system the radiation angle for various particles are calculated. When the angle has been measured one knows the identity of the particle. If there is no Cherenkov radiation one can exclude particles with masses lower than some limit.

5 Charged Higgs Events

In section 3 it was explained how the charged Higgs emerges as a result of adding an additional Higgs doublet. Below a description is given of the *events* we are looking for, that is what is happening with the charged Higgs bosons after they have been formed in an electron-positron annihilation. When the analysis is to be designed it is crucial to have exact knowledge of what one is searching for. To ease the reading, in the rest of the thesis a charged Higgs is sometimes referred to only as a Higgs.

5.1 The Topology of Higgs Events

With a branching ratio $B(H^{\pm} \to \tau\nu_{\tau}) = 1$ the Higgs events are quite simple and easy to classify. The most important decay channels of τ^- are

- $\mu^-\bar{\nu}_{\mu}\nu_{\tau}$, 17.7%
- $e^-\bar{\nu}_e\nu_{\tau}$, 18.0%
- $h^- \geq 0$ neutrals ν_{τ}, 49.8%
- $2h^-h^+ \geq 0$ neutrals ν_{τ}, 14.4%

where $h^{\pm}$ stands for $\pi^{\pm}$ or $K^{\pm}$[4].

From these numbers one finds that in 73% of the events there will be two charged particles, in 25% there will be four charged particles and in 2% there will be six charged particles. In other words, Higgs events are low multiplicity events.

In a Higgs event there will always be at least four neutrinos. Two from the decays of the Higgs particles and at least two from the tau decays. If the taus decay to leptons there can be up to six neutrinos. In other words there will be large missing momenta and energies. See fig. 2 for a sketch of the decay sequence.

Missing momenta give large acoplanarity angles, and this is perhaps the most useful characteristic of Higgs events apart from the low multiplicity. Another useful feature is the polar angle distribution. The cross section is proportional to $\sin^2\theta$ where theta is the angle between the beam axis and the direction of the Higgs particles. The differential cross sections of all the background processes have their largest values in the forward direction, that is with small θ.

5.2 The Cross Section of Higgs Events

One of the main problems when looking for charged Higgs particles is the small cross section. For energies between 130 and 192 GeV it will never exceed 0.6 pb for masses above 50 GeV. The first order expression is (see appendix A)

$$\sigma = M_W^4 G_f^2 \frac{(1-4M_H/s)^{\frac{3}{2}}}{24\pi s} \left(\frac{\cos^2 2\theta_w}{\cos^4 \theta_w} \frac{c_V^2 + c_A^2}{(1-M_Z^2/s)^2} + 16\sin^4\theta_w + 8\tan^2\theta_w \cos 2\theta_w \frac{c_V}{(1-M_Z^2/s)} \right).$$

See fig. 3 for a plot of the cross section as a function of $M_{H^\pm}$ and $\sqrt{s}$. It shows that higher energy does not necessarily give a bigger cross section.

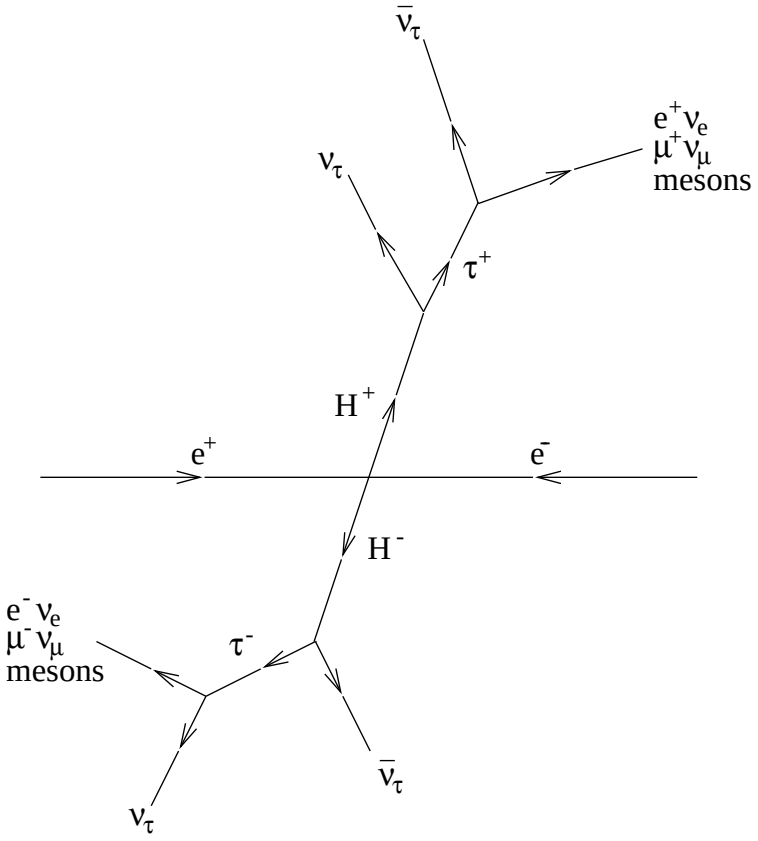

Figure 2: A Charged Higgs Event

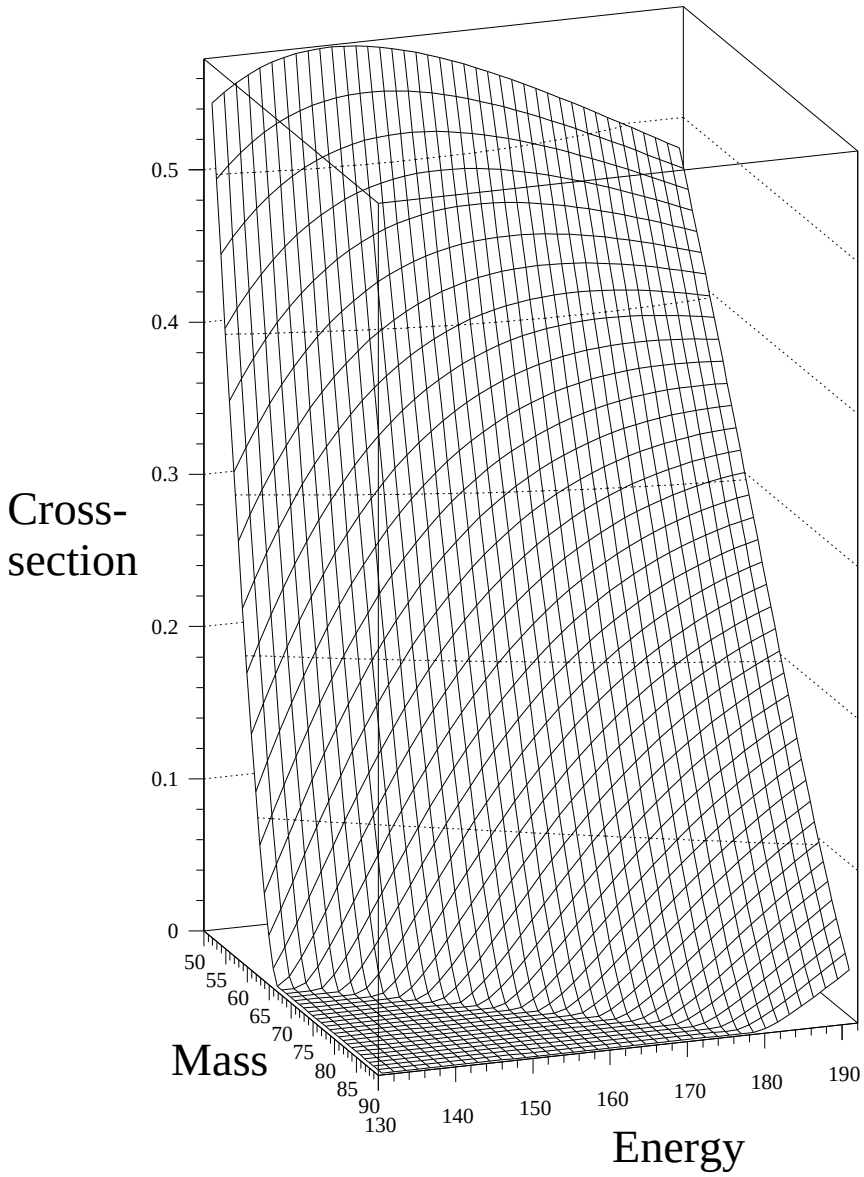

Figure 3: $\sigma_{H^\pm}$ as a function of E_{cm} and $M_{H^\pm}$.

6 Background Processes

With the increased energy at LEP2 there will be processes that did not exist at LEP1 or they had cross sections that were very small. Most important for this analysis is the W-pair production, $e^+e^- \to W^+W^-$, but also the processes $e^+e^- \to Z^0Z^0$, $e^+e^- \to Ze^+e^-$ and $e^+e^- \to We\nu$ have to be considered. In addition to these new processes we will have the familiar fermion anti-fermion production, the $\gamma\gamma$ production and the Bhabha scattering to contend with.

6.1 $f\bar{f}$ Production, $e^+e^- \to \gamma/Z^0 \to f\bar{f}$

Fermion-antifermion production is a process where the electron and positron annihilate to form a virtual photon or a Z^0-particle which subsequently decays to a fermion pair (See fig. 4). At LEP2 energies there will in most of these events be a hard ISR (Initial State Radiation) photon which lowers the center of mass energy so that an on-shell Z^0 is produced. The ISR photons are going very much in the forward/backward direction and in most cases they are not detected. In those events the remaining energy is $\frac{s+m_Z^2}{2\sqrt{s}}$. Otherwise the Z^0-particle is virtual with an energy equal to $\sqrt{s}$.

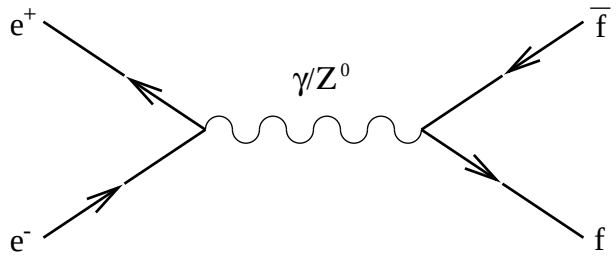

Figure 4: $e^+e^- \to \gamma/Z^0 \to f\bar{f}$

If the final state fermions are quarks, muons or electrons it is probable that most of the energy that is left after ISR is detected. For that reason such events are not a difficult background when searching for charged Higgs particles. The only fermion pairs that represent a problem are the tau pairs. If there is a hard ISR photon so that the total energy of the event is lowered such an event happen to resemble a charged Higgs event.

6.2 $\gamma\gamma$ Events

In a $\gamma\gamma$ event the initial electron-positron system radiates two photons[1] which form a new system consisting of a fermion pair: $e^+e^- \rightarrow e^+e^- + f\bar{f}$. Fig. 5 gives an example of the many diagrams contributing to the $\gamma\gamma$ cross section.

The invariant mass of this system is in most events very low, and the directions of the positron and electron after the radiation are very much along the beam direction. That means that in almost all these events the positron and electron are not detected. Another characteristic of these events is that the energy of the $\gamma\gamma$ system is rather low. Again the tau events are the most problematic. They tend to have higher transverse momenta and are more acoplanar.

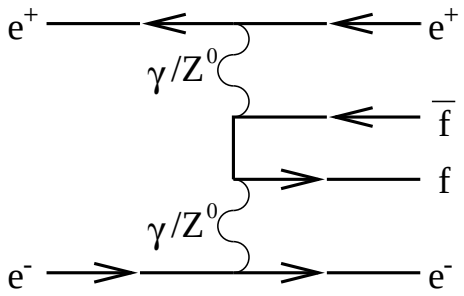

Figure 5: A $\gamma\gamma$ diagram

6.3 Bhabha Scattering, $e^+e^- \rightarrow e^+e^-$

Two diagrams give the major part of the Bhabha cross section. The annihilation diagram is included in the $f\bar{f}$ background, the scattering diagram is shown in fig. 6.

Even though shower formation is quite frequent in the forward direction due to the large amounts of material with which the electrons/positrons can interact, the Bhabha events represents no problem in this analysis. They are mentioned here because they have to be included when a preselection of the P3 data is compared to a sample of simulated events.

6.4 W-pairs

At LEP2 energies higher than twice the W mass will be reached, and for the first time W-pairs will be produced. See figure 7 for the lowest order Feyn-

[1]The electron and positron do not *radiate* photons in all the diagrams, but all the diagrams contain two internal photon lines.

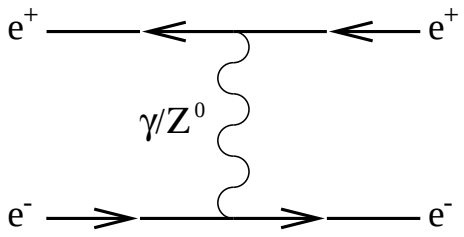

Figure 6: The Bhabha scattering diagram

man diagrams contributing to the cross section. When searching for charged Higgs particles decaying to taus and tau-neutrinos this is a disadvantage. If both the W particles decay to taus and tau-neutrinos the event has exactly the same signature as a charged Higgs event. The only difference is in the polar angle distribution. The differential cross section for Higgs production is proportional to $\sin^2\theta$ while the WW production is pointing more in the forward direction.

Hadronic decays and decays to muons and electrons are more easily dealt with. More of the energy is detected and in hadronic decays the events have small acoplanarity angles.

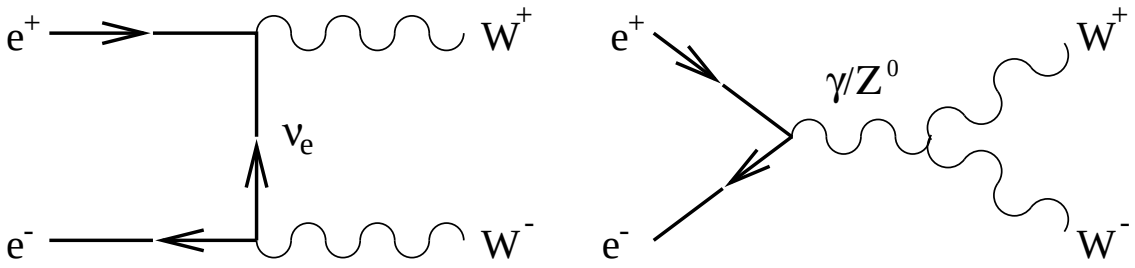

Figure 7: WW production diagrams

6.5 Z-pairs

As for the W-pairs, Z-pairs will be produced for the first time at LEP2. The Feynman diagrams are shown in figure 8. Z particles mostly decay to hadrons and the charged multiplicity is usually high, but there is a $3\frac{1}{2}\%$ chance for the Z to decay to each of the lepton pairs[4]. If one Z decays to a neutrino pair and the other decays to a tau pair, the event looks very much like a Higgs event.

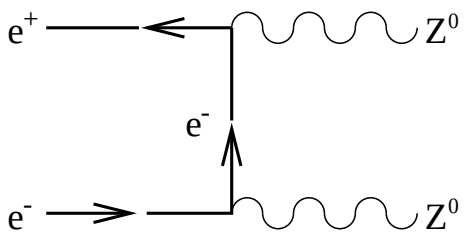

Figure 8: The ZZ production diagram

6.6 $We\nu$ and $Z^0e^+e^-$

Of these two backgrounds it is the $We\nu$ that is the most difficult. The neutrino takes away some of the momentum and energy and quite often the electron/positron is not detected. Fortunately the cross section is small, it is comparable the cross section for Higgs production.

Also in the $Z^0e^+e^-$ background the electron and/or the positron is often lost, but the Z's branching ratio to leptons is much smaller than it is for the W particle. That means that the charged multiplicity is mostly high, and the number of jets tends to be greater than two.

6.7 Cross Sections

The total cross sections for background processes are generally much bigger than the signal cross section. The numbers are given in table 3. Cross sections for the various $\gamma\gamma$ channels are not included. They are extremely large, and when simulations are done only a subset of the phase space is explored. As an example, the DST's containing $\gamma\gamma \to$ hadrons produced according to the VDM model only have events were the polar angle of the charged tracks is larger than 15 degrees, the minimum momentum of the tracks is larger than 0.2 GeV and the invariant mass of the two-photon system is larger than 2 GeV. The cross section for this channel with these limitations is 6.1 nb.

	ff	W^+W^-	Z^0Z^0	$We\nu$	$Z^0e^+e^-$
136	401	0.5	0.45	0.09	6.0
161	228	3.4	0.46	0.53	6.4
175	174	15	0.47	0.65	6.6
192	134	18	1.2	0.90	6.7

Table 3: Background Cross Sections in pb^{-1}.

As one can see from the table, in this energy region the cross section for $f\bar{f}$ decreases with increasing energy while the opposite is true for the other processes. W-pair and Z-pair production have a steep climb at threshold energies.

The cross section for the $f\bar{f}$ production is very much larger than the other cross sections. This means that even though the fraction of dangerous tau pairs from $f\bar{f}$ is small, the $f\bar{f}$ background gives some irreducible background. As for the W-pairs, this is not a problem before the energy is above 160 GeV. At higher energies it is the most important background.

7 Analysis

As described earlier the main characteristics of a Higgs event with tau-decays are the low multiplicity, the missing momenta giving acoplanarity and the missing energy. In this analysis these characteristics are exploited when removing background events.

7.1 Simulations

When designing and testing this analysis it is necessary to do simulations. Working with real data one can never know with certainty which kind of event has occurred. The plots presented in this section are all results of simulations.

The first step is to simulate the physics before anything is measured in the detector, i.e. the processes we wish to investigate. This is done with *event generators*. Most of the events were produced with PYTHIA[33] and TWOGAM[25].

The next step is to simulate what happens in the detector, what is really *measured*. DELSIM[26] is taking care of that part and is giving "Raw Data" as output with the same format as real DELPHI data. Finally DST's[27] (Data Summary Tapes) are produced by DELANA[28]. They can be read with the help of PHDST[29], a program package written in order to ease the access to data.

In an analysis designed to find rare events like Higgs events it is important that all backgrounds are minimized. Estimating small remaining backgrounds takes quite a lot of simulation as the relative uncertainty is large for small numbers. In particular if zero events pass the cuts and the cross section is large there is a problem. If the true expectation value is 1, 2 or 3 the chance for finding zero events is 0.368, 0.135 and 0.050[30], i.e. it is not unlikely that the expectation value *is* 1,2, or 3 when zero events are observed. Therefore it is important to do enough simulations so that the uncertainty is scaled down. The uncertainty is scaled down if the equivalent integrated luminosity of the simulations are higher than the real integrated luminosity.

The problem of doing numerous simulated events is that it can take several minutes to do the calculations of one single event. In other words it is a question of available computing resources. For this analysis only the signal events were produced in Oslo. Even though the signal events are of low multiplicity and the number of events simulated is not very high, it took several weeks to produce the DST's.

7.1.1 $\gamma\gamma \rightarrow$ hadrons

The interactions between two photons leading to hadronic final states are described by combining contributions from three different models: the Vector Dominance Model (VDM), the Quark Parton Model (QPM) and the QCD model[31].

The VDM model describes the interaction between bound state vector mesons. The $\gamma\gamma$-system of the events generated according to this model mainly have low four momentum transfer (Q^2) and low transverse momenta. The QPM model assumes direct (QED) coupling of the photons to a quark pair, and describes higher momentum transfer photons than the VDM model. In the QCD model one or both of the photons is resolved into partonic constituents. This model has the highest invariant masses and transverse momenta.

7.2 Quality Cuts

Unfortunately it is not unusual for spurious events to resemble Higgs events. Before inventing cuts to eliminate the background already described, spurious events have to be taken care of. Spurious events are events not originating from collisions between the accelerated electrons and positrons. This could be beam gas events where accelerated particles have hit some of the few gas particles in the beam pipe, beam wall events were electrons/positrons have hit the wall of the beam pipe or it could be cosmic events, radiation from outside. Another problem is the resolution of the detector. For example, the relative error in calorimeters is proportional to $\frac{1}{\sqrt{E}}$ meaning that the relative error is large for small energies. To overcome these difficulties some preliminary quality cuts are applied.

In a typical spurious event the particles do not come from the collision spot of the experiment. Variables commonly used as measures of this property are the *impact parameters*, $b_{r-\phi}$ and b_z. As shown in figure 9 $b_{r-\phi}$ is defined as the smallest distance from the particle trajectory to the beam spot in the $r-\phi$ plane, b_z as the smallest distance in the z direction, the direction parallel to the beam direction.

First all tracks with $p < 1\ GeV$ are removed from the event. In this analysis it is not very important that this limit is set so that energy of the event can be measured with the best possible accuracy. What matters is whether there *are* large missing energies or not.

Secondly it is demanded that for all the remaining charged tracks

- the impact parameter in the $r-\phi$ plane, $b_{r-\phi}$, be less than 2 cm,

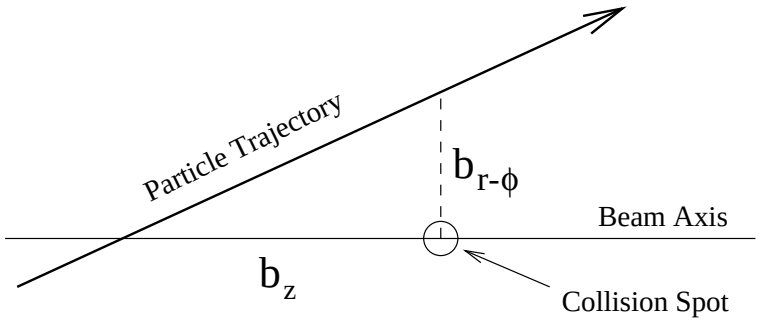

Figure 9: Definitions of $b_{r-\phi}$ and b_z.

- the impact parameter in the z (beam) direction, b_z, be less than 6 cm
- and the track length be greater than 50 cm.

If only one of the charged particles doesn't fulfill these requirements the whole event is rejected. The reason for not just removing the charged particles that are not OK, is that the Higgs events have low multiplicity and the charged particles are usually energetic and thereby well detected. If there is something wrong with one of the charged particles it is therefore probably not a Higgs event. The limits of $b_{r-\phi}$ and b_z have been fixed by comparing real data and simulations, see section 9.1. Finally, an upper limit is set on the absolute value of the total charge of the event, $|C| < 2$, to ensure that not more than one charged particle is lost.

7.3 Jet Reconstruction

Since all the final state particles in a Higgs event come from the tau decays, they will most likely form two well separated jets. It is therefore demanded that a Higgs candidate event should contain exactly two jets.

In this analysis the LUCLUS routine is used, a part of the JETSET package[24], for the jet reconstruction. The basic idea of the algorithm is to assign to each pair of particles i and j a "distance" d_{ij}. The distance measure used in LUCLUS is

$$d_{ij}^2 = \frac{1}{2}\left(|\vec{p_i}||\vec{p_j}| - \vec{p_i}\cdot\vec{p_j}\right)\frac{4|\vec{p_i}||\vec{p_j}|}{(|\vec{p_i}|+|\vec{p_j}|)^2} = \frac{4|\vec{p_i}|^2|\vec{p_j}|^2\sin^2(\theta_{ij}/2)}{(|\vec{p_i}|+|\vec{p_j}|)^2}$$

where $\vec{p_i}$ and $\vec{p_j}$ are the momenta of the the particles and θ_{ij} is the angle between them. For small θ_{ij} $\sin(\theta_{ij}/2) \approx \frac{1}{2}\sin\theta_{ij}$ and $\cos\theta_{ij} \approx 1 \Rightarrow (|\vec{p_i}| +$

$|\vec{p_j}|)^2 = |\vec{p_i}|^2 + |\vec{p_j}|^2 + 2|\vec{p_i}||\vec{p_j}| \approx (\vec{p_i} + \vec{p_j})^2$ and the expression is reduced to

$$d_{ij} \approx \frac{|\vec{p_i} \times \vec{p_j}|}{|\vec{p_i} + \vec{p_j}|}.$$

In this limit the distance measure is equal to the transverse momentum of either of the particles with respect to the direction of the sum of the two momenta. If the particles are back-to-back d_{ij} is more related to the invariant mass.

Initially all the particles are assumed to be a cluster by themselves. Then the two clusters with the smallest d_{ij} are found, and if d_{ij} is smaller than d_{join} which is set by the user, the two clusters are joined to one. This is repeated until all the d_{ij} are greater than d_{join}.

After a joining and the corresponding calculation of the new cluster momentum, it might be that some particles belonging to this cluster actually are closer to some other cluster. Because of this a reassigning procedure has to be done for every joining.

When this routine is used in an analysis treating real data the momenta, the $\vec{p_i}$'s, are the momenta associated with reconstructed tracks. It is not correct to call them "particle momenta" as the momenta stored in the DST's are the momenta calculated from measurements in the detector. More precisely they can be called "track momenta".

The setting of the d_{join} value is rather important as it determines the number of jets LUCLUS will form. When looking for hadronic jets it has been customary to use $d_{join} = 5$ with LEP2 energies[32]. However, when the charged Higgs particles decay to taus and neutrinos the visible energy is halved and besides the tau events tend to have small jet opening angles. Therefore a smaller value can be used. Using the same sample of simulated charged Higgs events $d_{join} = 4$ GeV gives 630 two-jet events, $d_{join} = 2.5$ GeV gives 687 and $d_{join} = 1$ GeV gives 719.

A smaller value will give more Higgs events with two jets, but as can be seen in fig. 10 the extra two-jet events gained have small angles between the two jets. To ensure that possible Higgs candidates have well separated jets d_{join} should therefore not be set too low. Taking into account both the number of jets and the angles between the jets $d_{join} = 2.5$ GeV have been chosen.

Figure 11 shows a frequency plot of the number of jets in some background channels and in the signal. As expected only a few percent of the signal is rejected by demanding two jets. In this plot it seems to be quite an effective cut, especially in the W-pair and in the Z-pair backgrounds, but of course the number of jets is correlated to other variables, as the acoplanarity angle, and it is not crucial to the analysis as a cut by itself.

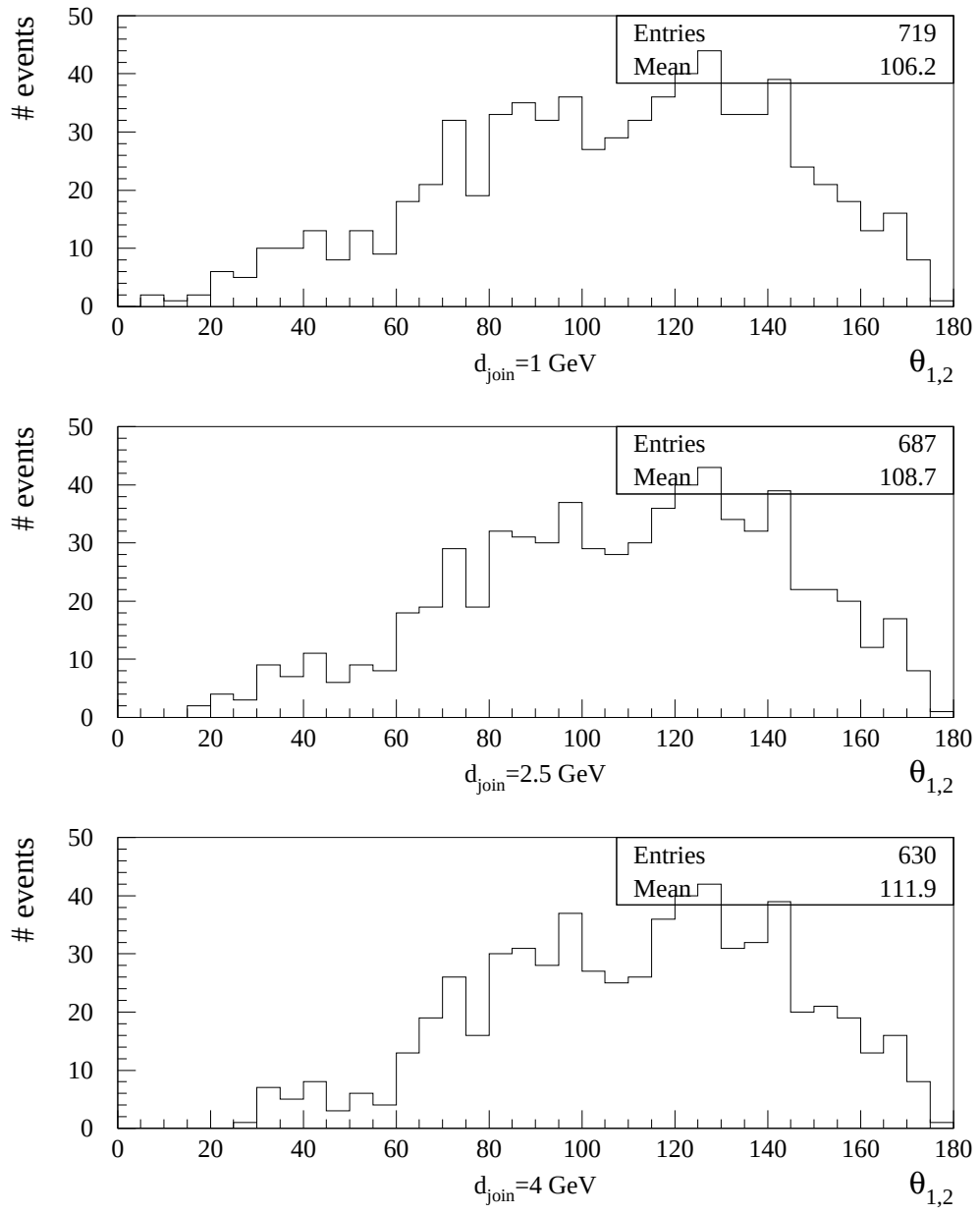

Figure 10: Plots of the distribution of the angle between the jets in two-jet Higgs events, $\theta_{1,2}$. The same sample of H^+H^- events (1000 events with $m_H = 60$ GeV, $\sqrt{s} = 161$ GeV) have been used in all the plots and as can be seen the number of two-jet events increases as d_{join} gets smaller. At the same time the number of events with small angles between the jets also increases.

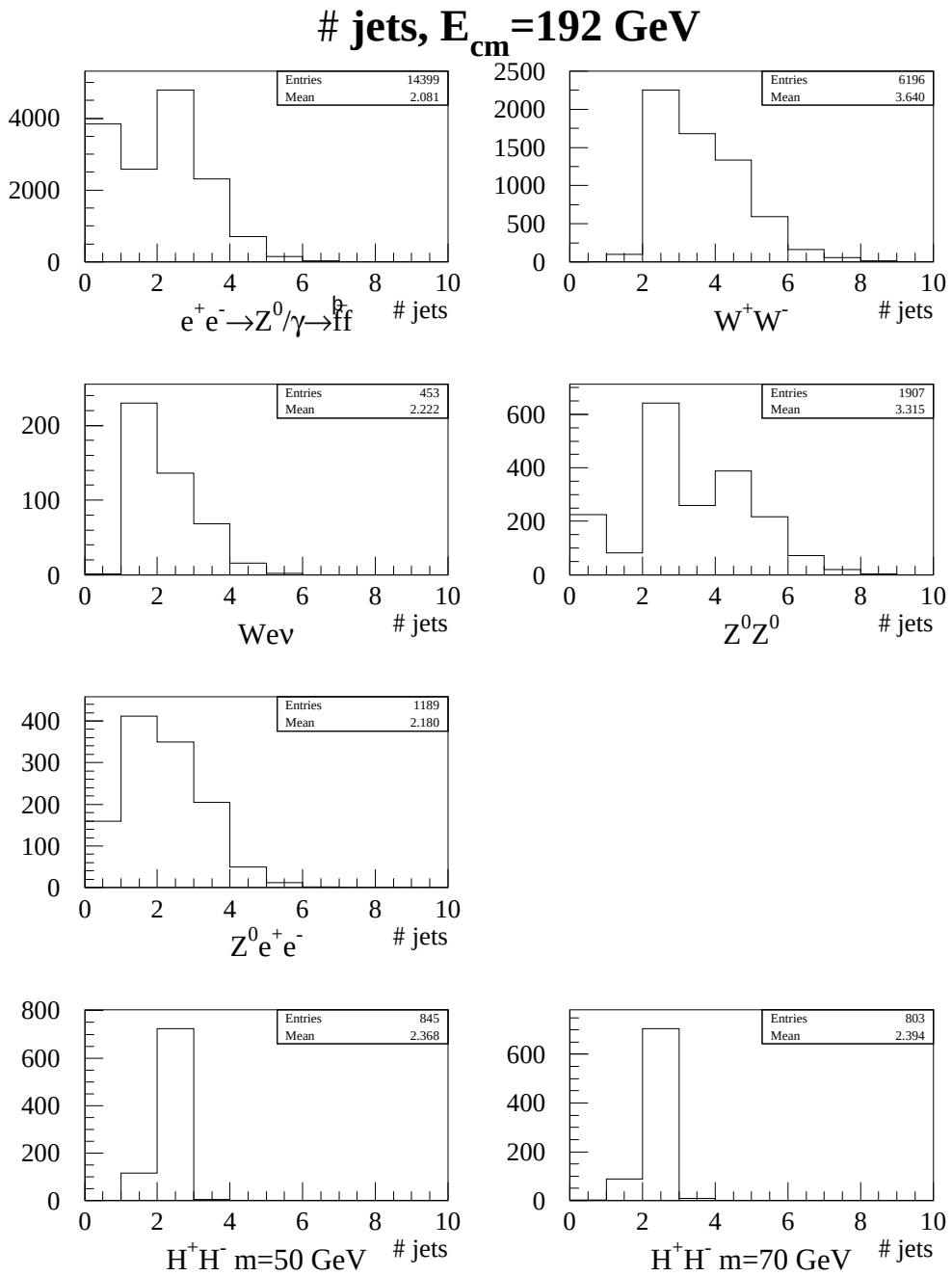

Figure 11: The number of jets in background and signal events after the quality cuts have been implemented.

However, when the two-jet events have been selected one can demand that each jet should contain at least one charged particle. This is natural as the jets both originate from a charged Higgs particle. The total charged multiplicity is to be less than 7. Another reason to select the two jet events is that it is easy to define the acoplanarity in terms of the jet axes.

7.4 Thrust Axis and Angle

In the LUTHRUST routine, also a part of the JETSET package, the thrust T is defined by

$$T \equiv \max_{|\vec{n}|=1} \frac{\sum_i |\vec{n} \cdot \vec{p_i}|}{\sum_i |\vec{p_i}|}$$

and the thrust axis is defined as the $\vec{n}$ vector for which the maximum is obtained[34]. As one can see T is the sum of the projections of the momenta onto the thrust axis divided by the scalar sum of all the momenta. A two-jet back-to-back event gives $T \approx 1$ while an isotropic event gives $T \approx \frac{1}{2}$. The thrust axis represents an average direction of the event.

As mentioned earlier the differential cross section for charged Higgs production is proportional to $\sin^2\theta$ (see appendix A) while the background is pointing more in the forward direction. That makes it natural to put an upper limit on the *thrust angle*, the angle between the thrust axis and the beam axis.

This cut is most effective on the various $\gamma\gamma$ channels as they are very much peaked in the forward direction, especially the hadronic. In figure 12 one can see that most of the hadronic and a substantial part of the leptonic $\gamma\gamma$ events are removed by setting the upper limit for $|\cos\theta|$ to 0.85. However, as will be shown later this cut is actually not crucial for the removal of two-photon events. It turns out that it is more important in the W- and Z-pair channels.

7.5 Acoplanarity

In the analysis the acoplanarity angle ϕ is defined as follows: Let each of the jet momenta, $\vec{p_1}$ and $\vec{p_2}$, form a plane with the beam axis. The acoplanarity angle is then the angle between these two planes. See fig. 13. It is a measure of the "twisting" of the event. An equivalent definition is to let ϕ be equal to the angle between $\vec{p_1}$ and $\vec{p_2}$ in the $R - \phi$ plane. See fig. 14.

As can be understood from the definition a perfectly reconstructed event where all the particles have been detected and all the particle trajectories

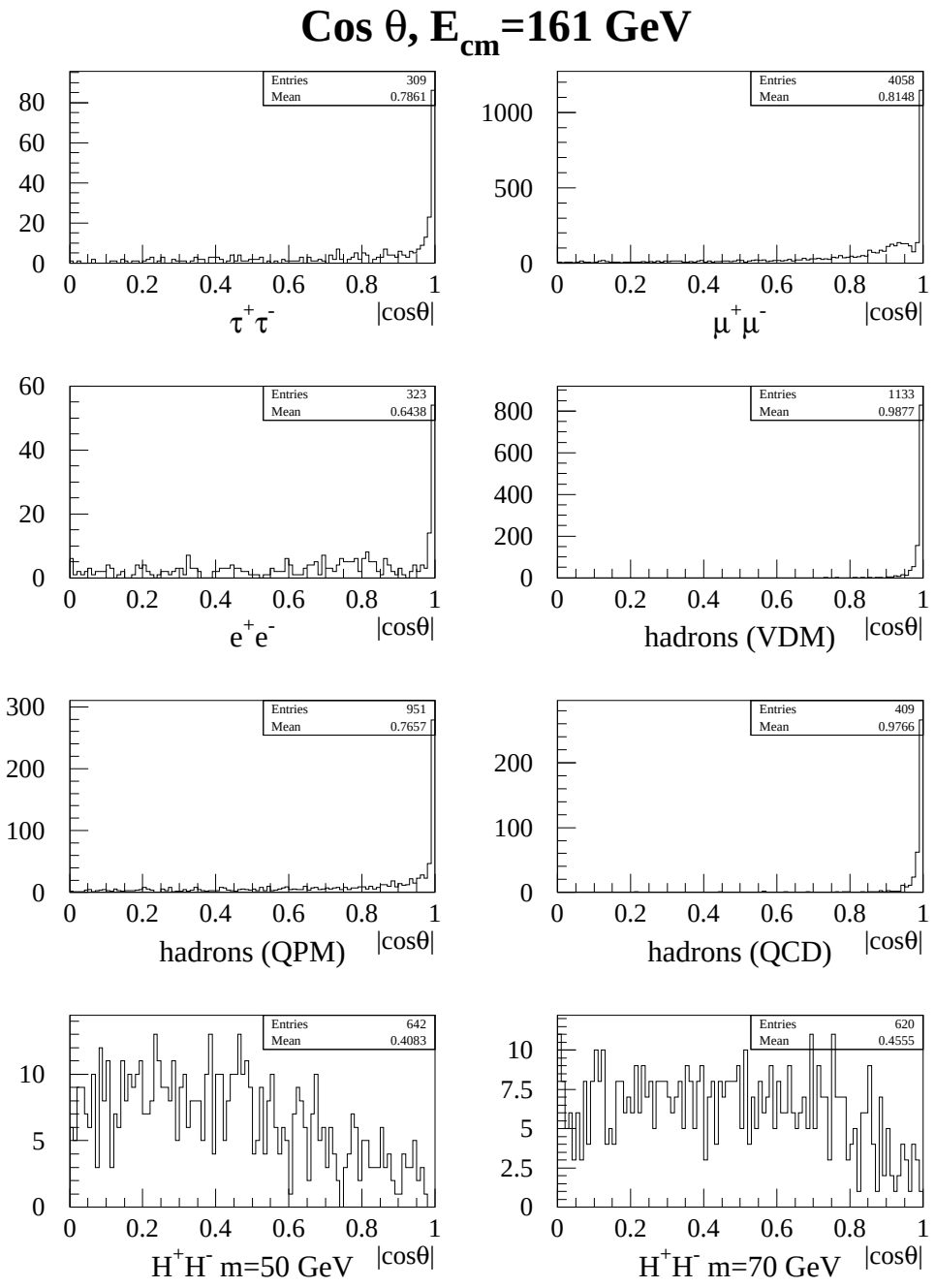

Figure 12: The $|\cos\theta|$ distribution for the various $\gamma\gamma$ channels and for the signal with Higgs masses of 50 and 70 GeV. The events used in this plot have two jets with at least one charged particle.

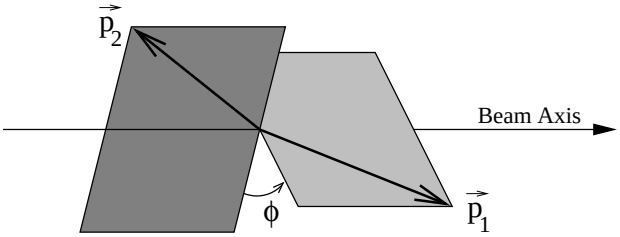

Figure 13: Acoplanarity

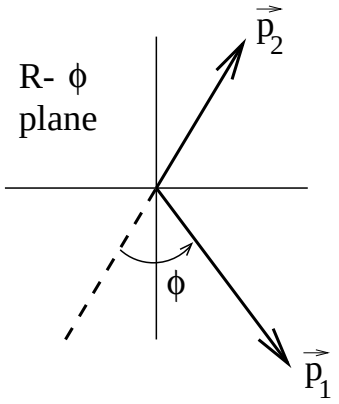

Figure 14: Acoplanarity

are correct will have an acoplanarity angle equal to 0. If there are missing momenta which is typical for a Higgs event with taus, the two jets will not lie in the same plane and the acoplanarity angle will be non-zero.

Figure 15 shows that only a couple out of several thousand $f\bar{f}$ events are left with a cut on 20°. Unfortunately this cut takes away a substantial part of the signal, but is too crucial to be omitted. As can also be seen it is a harder cut with small $M_H = 50GeV$ than with $M_H = 70GeV$. The reason is that Higgs particles with small masses have larger momenta, and the decay, which is isotropic in the center of mass system, will tend to point in the direction of the Higgs particle. Figure 16 shows the same plot for two-photon events.

7.6 Transverse Momentum

A lower limit on transverse momentum rejects events with small polar angles and low energy. A typical $\gamma\gamma$ event possesses both these characteristics and all of the events that remain after the cuts on polar angle and acoplanarity are rejected by this cut which has been set to 8.5% of the center of mass energy. The transverse momentum is defined by

$$p_t = \sum_{i=1}^{2} p_i \sin\theta$$

where p_i is the momentum of jet i. See fig. 17.

7.7 Energy Distributions

Background left after the cuts discussed so far is mostly leptonic W-pairs. If both the W's decay to taus (happens in 1.17% of the WW events[4]) the

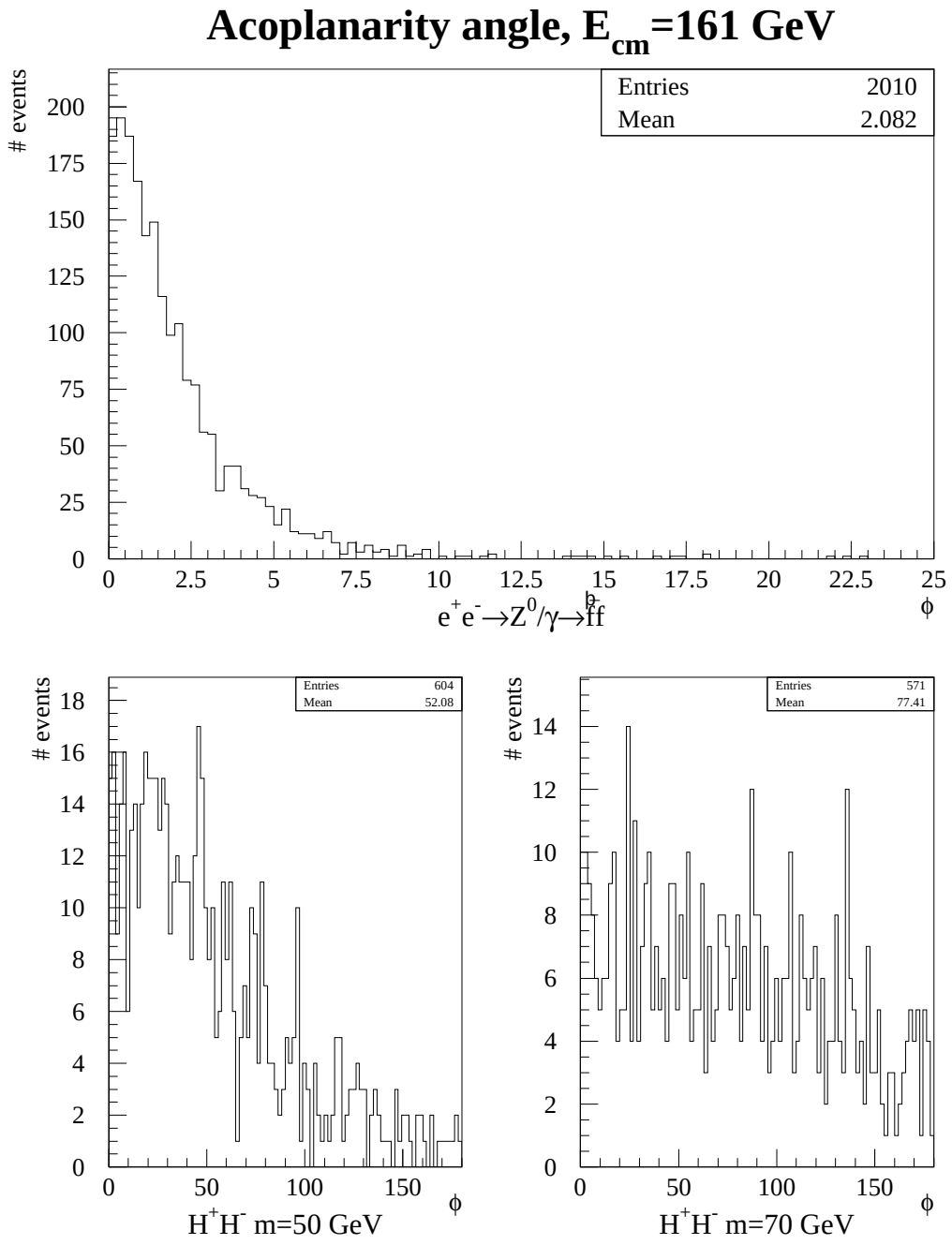

Figure 15: The ϕ distribution in $f\bar{f}$ and Higgs events. The events used in these plots have two jets with at least one charged particle.

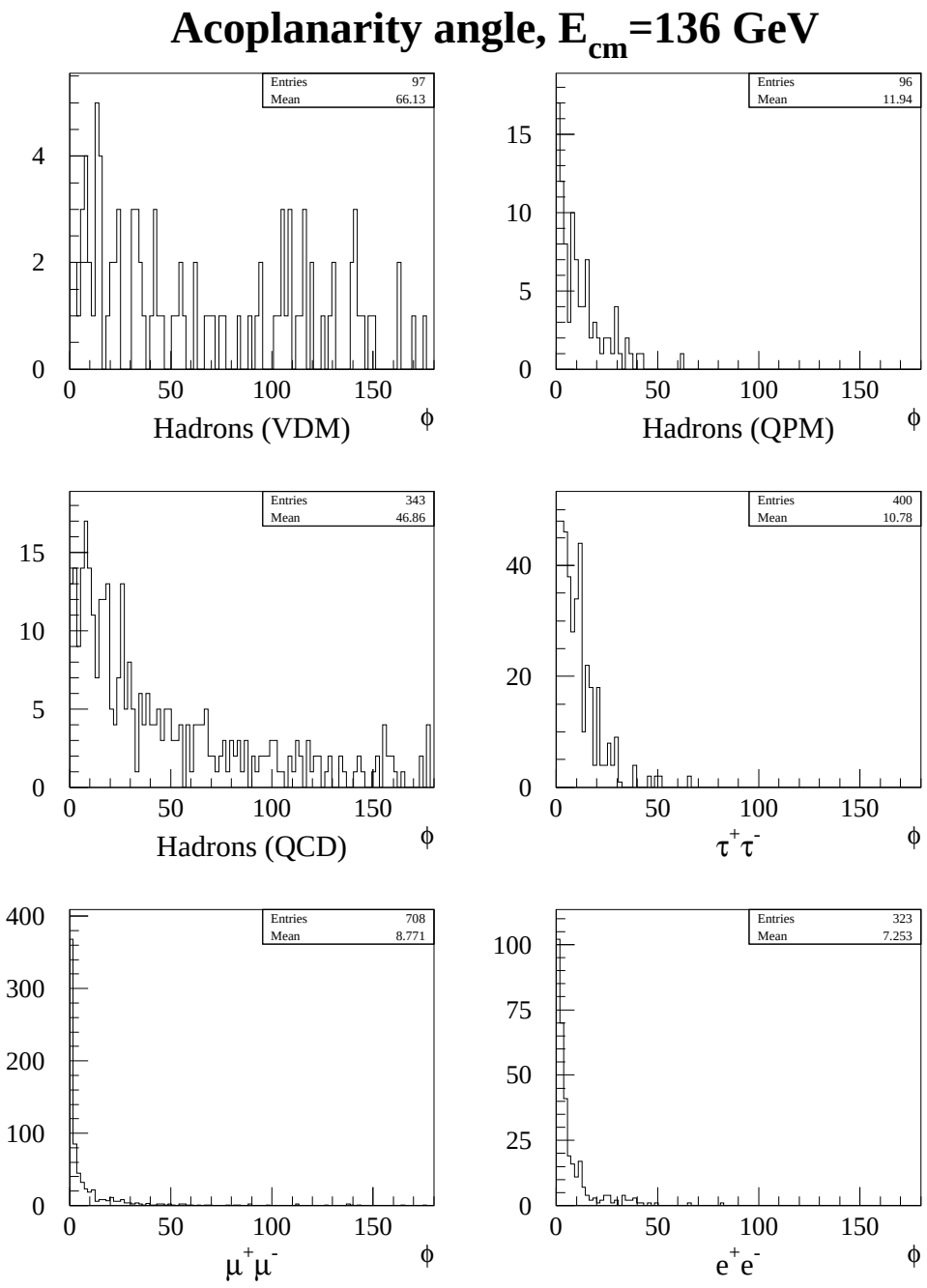

Figure 16: The ϕ distribution in two-photon events. The events used in these plots have two jets with at least one charged particle.

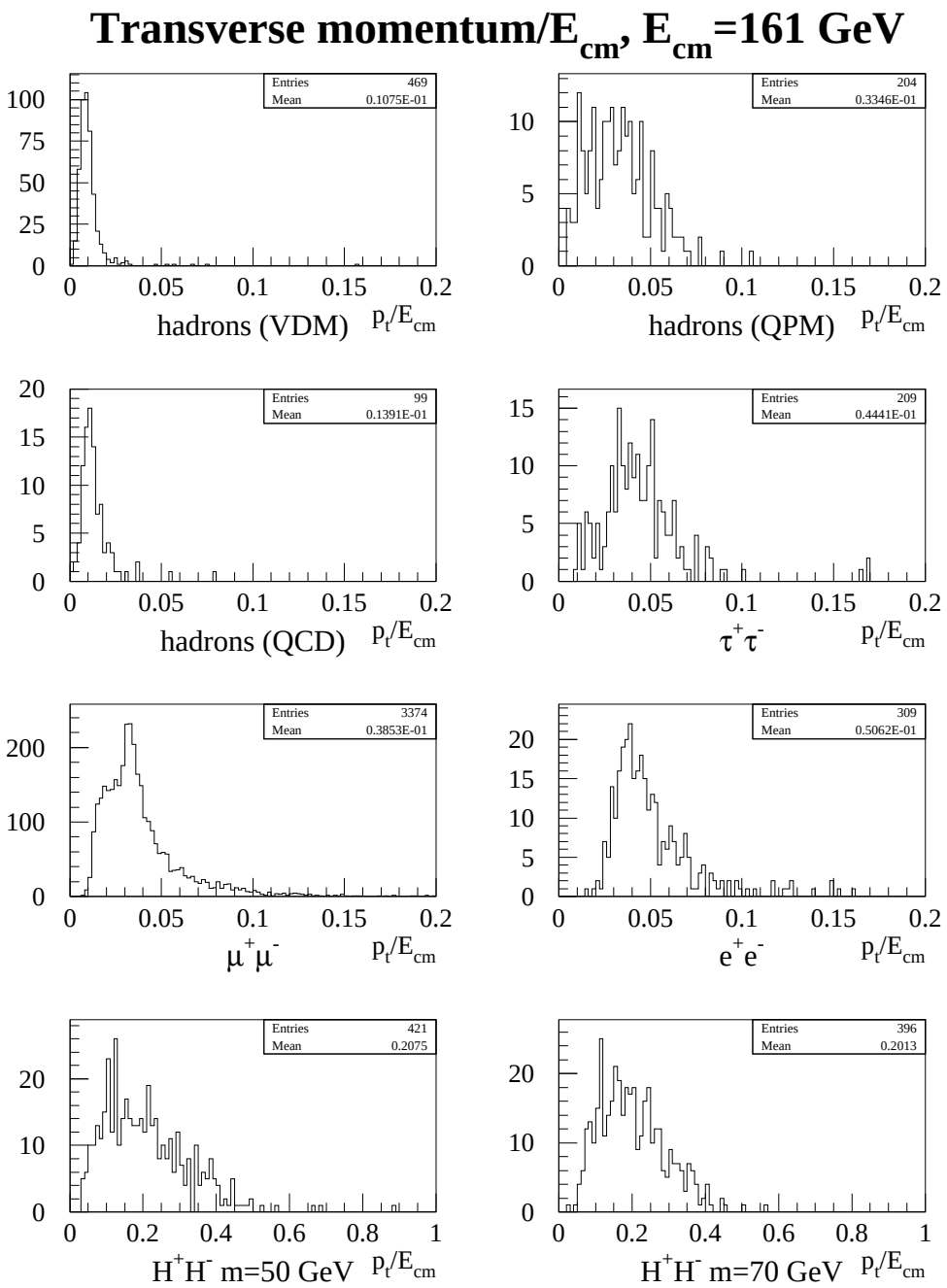

Figure 17: The p_t distribution in $\gamma\gamma$ and Higgs events. The events used in these plots have two jets with at least one charged particle.

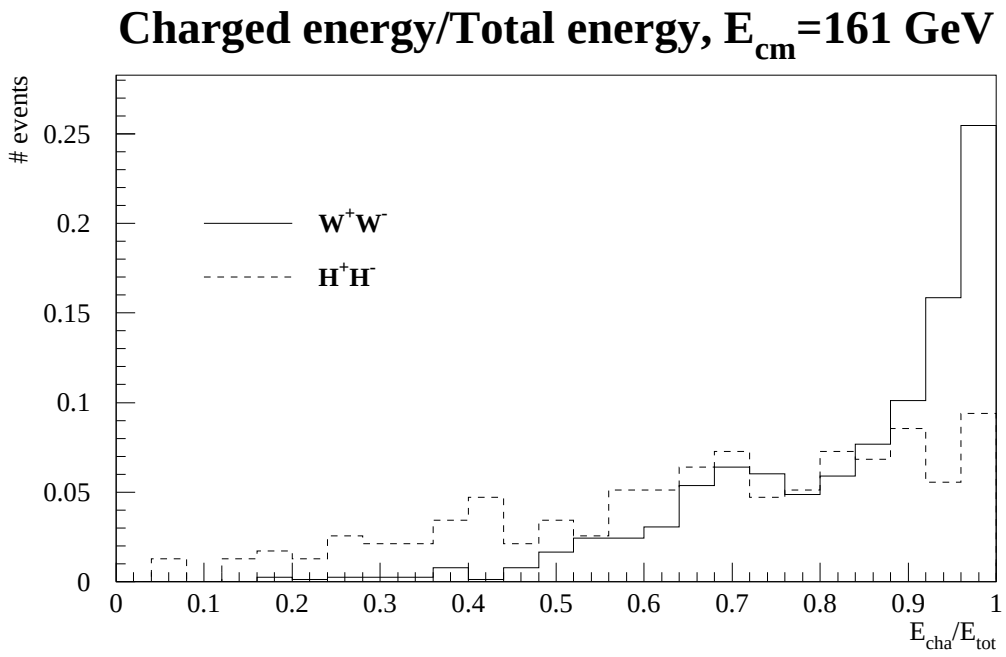

Figure 18: Frequency plot of the fraction of charged energy in the total energy. Only two-jet events with total energy higher than 1/4 of E_{cm} and with at least one charged particle in each jet are included. They also have to pass the cuts on $|\cos\theta|$ and ϕ.

event looks exactly like a Higgs event and anything that is done to remove these events will remove Higgs events with the same probability. If one or both of the W's decay to an electron or a muon there is one or two neutrinos less than in a Higgs event, and thereby a higher visible energy. In such an event the visible energy is all charged energy, there are no neutral particles.

In Higgs events with $Br(H^{\pm} \to \tau\nu) = 1$ there will in more than 50% of the cases be neutrals. Due to this the peaks in the distributions in charged energy for signal and W-pairs are better separated than in the distribution of total energy. It has therefore been chosen to have a cut in charged energy rather than in total energy.

Fig. 18 shows the distribution of the ratio between charged energy and total energy, and as one can see the fraction of charged energy is higher in W-pairs than in Higgs events. Only the events with total energy higher than 1/4 of the center of mass energy are included as events with lower energy are of no interest. The upper limit on charged energy has been set equal to

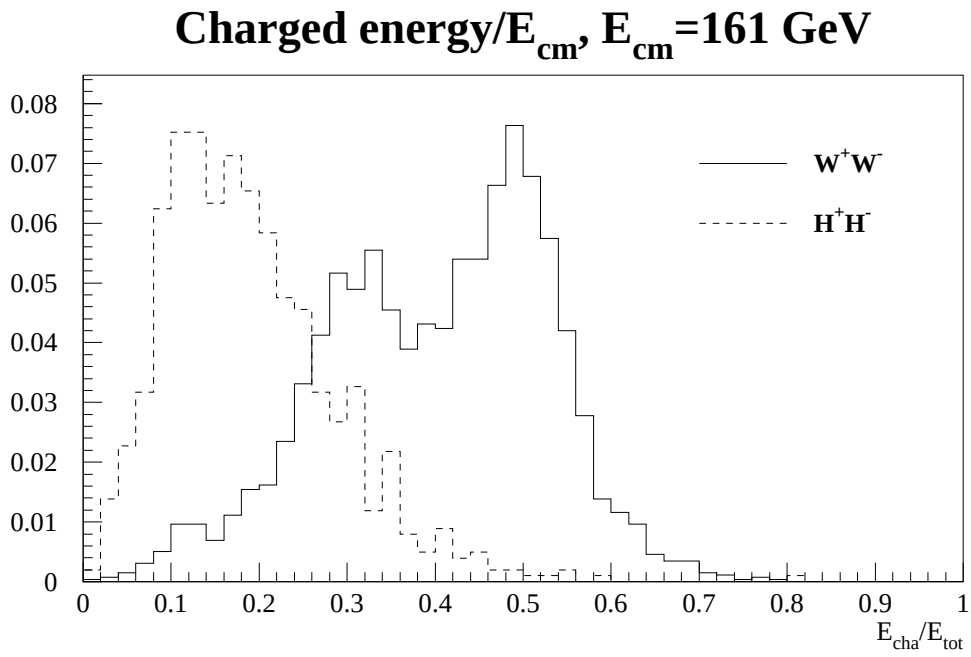

Figure 19: Frequency plot of charged energy divided by E_{cm}. Only two-jet events with at least one charged particle in each jet are included.

1/4 of the total energy and as fig. 19 shows this removes most of the W-pair background.

The simulations show that all the $\gamma\gamma$ background is removed with the cuts described so far, but very large cross sections make it difficult to do enough simulations to get sufficient statistics. A lower bound on the charged energy is set so that one can be more confident that no $\gamma\gamma$ events slip through.

Events with ordinary tau pairs decaying to hadrons occasionally have low charged energies but high neutral energies. To get rid of these a rather loose cut on the total energy, $E_{tot} < 45\%$ of E_{cm}, has been applied.

With center of mass energies lower than threshold energy for W-pair production, it is unnecessary with a hard cut on charged energy. At P3 energies the cut is loosened up to a limit of 3/8 of E_{cm}. The idea behind this lower bound is that tau pairs decaying to hadrons can give charged energies of about one half the center of mass energy, and to be sure they are removed the limit is set somewhat lower.

The final demand is that the deposited energy in the forward/backward 30° cones has to be lower than 7% of the center of mass energy. The purpose

is to reject poorly reconstructed events in the forward region.

7.8 Summary of Cuts

To summarize the results from this discussion of how to search for charged Higgs bosons, a list of the cuts are given below. It is meant to give the reader an easy access to the exact details of the analysis.

In all detectors there will be noise and the resolution is not infinite. Therefore all tracks with

- all $p < 1$ GeV

are removed from the events. To remove cosmics, beam wall and beam gas events the remaining charged tracks are demanded to have

- $b_{r-\phi} < 2$ cm
- $b_z < 6$ cm
- $l_{track} > 50$ cm

To ensure that not more than one charged particle is lost

- $|Q| < 2$

where Q is the total charged of the event. After these quality cuts the rest of the cuts can be implemented. They exploit the characteristics of charged Higgs events: two jets with at least one charged particle, low multiplicity, missing momenta and energy and large polar angles.

- $N_{jets} = 2$
- $N_{cha,1} \geq 1$, $N_{cha,2} \geq 1$
- $N_{cha} < 7$
- $|\cos\theta| < 0.85$
- $\phi < 20^\circ$
- $p_t > 8.5\%$ of $\sqrt{s}$
- $E_{\theta<30^\circ} < 7\%$ of $\sqrt{s}$
- 4% of $\sqrt{s} < E_{cha} < \frac{1}{4}\sqrt{s}$ ($\frac{3}{8}$ if $\sqrt{s}$ is less than W-pair threshold.)
- $E_{tot} < 45\%$ of $\sqrt{s}$

N_{jets}: number of jets, $N_{cha,n}$: charged multiplicity of jet n, N_{cha}: total charged multiplicity, θ: angle between thrust axis and beam axis, ϕ: acoplanarity angle, p_t: transverse momentum, $E_{\theta<30^\circ}$: energy in forward/backward 30° cones, E_{cha}: total charged energy, E_{tot}: total measured energy.

8 Results from Simulations

In the previous section an analysis was designed to find charged Higgs bosons. Now that the exact cut values are ready one can estimate the background problems and expected signals. This is accomplished with the aid of simulations. Ideally, development and testing of the analysis should be done with independent samples of simulated events. However, as already mentioned, doing simulations takes a lot of computing resources, so the same set of DST's are used for both tasks.

The results from simulations are summarized in tables 4-8. The columns contain the total numbers of simulated events, the equivalent integrated luminosities, the number of events passing all the cuts, the corresponding fractions, the cross sections and the number of background events expected with the integrated luminosity given on top of each table.

As already mentioned it is important to do enough simulations so that the uncertainty in background is small. Unfortunately it has not been possible to find enough/any simulations for all the two-photon channels with the various center of mass energies. It is only at $\sqrt{s} = 161$ GeV that the numbers of Monte Carlo two gamma events are satisfactory, but even at that energy one channel is missing, the $e^+e^- \to e^+e^-e^+e^-$ channel.

At $\sqrt{s} = 161$ GeV none of the $\gamma\gamma$ channels seem to give any background at all. This is also the case with $\sqrt{s} = 136$ GeV, but those results cannot be given much weight as the corresponding luminosities are quite low. Anyway, when estimating the total expected background a two-photon background equal to zero is assumed for all the center of mass energies. This eliminates the problem of overlap between the various hadronic simulations, QCD, VDM and QPM.

As the events are independent it is natural to use binomial statistics. The number of expected real events of a particular kind is thereby estimated by

$$N_i = \frac{N_{b,i}}{N_{s,i}} \sigma_i \int Ldt$$

where $N_{s,i}$ is the number of simulated events, $N_{b,i}$ is the number that passed the cuts and σ_i is the cross section. The total background is

$$N = \sum_i N_i.$$

The uncertainty in background i is

$$\Delta N_i = \frac{\sigma \int Ldt}{N_s} \sqrt{N_b \left(1 - \frac{N_b}{N_s}\right)}$$

Simulations with $\sqrt{s} = 192$ GeV, $\int L\,dt = 300pb^{-1}$						
Channel	MC events	$\int Ldt$ (pb^{-1})	After cuts	Fraction (%)	σ (pb)	# events
Background						
ff	37827	282	3	0.0079	134	3.2 ± 1.8
W^+W^-	27933	1551	188	0.67	18	36 ± 3
Z^0Z^0	8651	7209	51	0.59	1.2	2.1 ± 0.2
$We\nu$	1000	1111	7	0.70	0.90	1.9 ± 0.7
$Z^0e^+e^-$	3220	481	1	0.031	6.7	0.62 ± 0.62
Total background						44 ± 4
Signal						
$M_H = 50$	1000	2083	270	27	0.48	39 ± 2
$M_H = 60$	1000	2702	286	29	0.37	32 ± 2
$M_H = 70$	1000	4000	299	30	0.25	22 ± 1
$M_H = 80$	1000	7692	301	30	0.13	11 ± 0
$M_H = 90$	1000	30303	301	30	0.033	3.0 ± 0.0

Table 4: Results from simulations with $\sqrt{s} = 192\,GeV$. The last column is the expected number of events corresponding to $300pb^{-1}$.

and the total uncertainty is given by

$$\Delta N = \sqrt{\sum_i (\Delta N_i)^2}.$$

Tables 4-6 show that for $\sqrt{s} \geq 161$ GeV the W-pair background is the most important one, especially for 175 and 192 GeV. The W-pair cross section has a steep climb around twice the W mass and the fraction of tau decays is not changing with varying energy so this is not hard to understand.

The behaviour of the W-pair cross section suggests that the best center of mass energy to look for charged Higgs particles with masses of 50 or 60 GeV is somewhat below the W-pair threshold. Also the cross section is actually larger with $\sqrt{s} = 160$ GeV than for higher energies with such masses. For higher masses the cross section is small, and the center of mass energy has to be raised.

Another aspect worth noticing is that higher masses give higher efficiencies, more of the Higgs events passes the cuts if the mass is high. Unfortunately the cross section drops dramatically when the mass approach half the center of mass energy.

Simulations with $\sqrt{s} = 175$ GeV, $\int L\,dt = 300pb^{-1}$						
Channel	MC events	$\int Ldt$ (pb^{-1})	After cuts	Fraction (%)	σ (pb)	# events
Background						
ff	34154	196	2	0.0058	174	3.1 ± 2.2
W^+W^-	5017	334	41	0.82	15	37 ± 6
Z^0Z^0	1500	3191	12	0.80	0.47	1.1 ± 0.3
$We\nu$	1746	2686	12	0.69	0.65	1.3 ± 0.4
$Z^0e^+e^-$	1715	260	1	0.058	6.6	1.1 ± 1.1
Total background						44 ± 7
Signal						
$M_H = 50$	1000	1887	298	30	0.53	47 ± 2
$M_H = 60$	1000	2702	302	30	0.37	34 ± 2
$M_H = 70$	1000	4761	315	32	0.21	20 ± 1
$M_H = 80$	1000	15625	324	32	0.064	6.2 ± 0.3

Table 5: Results from simulations with $\sqrt{s} = 175\,GeV$. The last column is the expected number of events corresponding to $300pb^{-1}$.

8.1 Impact of the Various Cuts

When designing an analysis one looks at the various distributions and if there is a difference between signal and background a cut can be done. But this method does not take into account the correlations between the variables in which the cuts are made. It is of course possible to make scatter plots and in that way examine the correlation between two variables. However, there is often a connection between more than two variables, and it is getting very complicated. To really see the importance of a cut, to see if the cut really does any good, the cut should be applied as the last one, and the impact can be evaluated.

Tables 9-11 give the number of events removed by the individual cuts with the cut in question applied as the last one, i.e. after the other cuts have been applied. The cuts in $\cos\theta$ and $E_{\theta<30^\circ}$ are treated as one cut as they are expected to be very much correlated. This is also the case for p_t and E_{cha}. When compared with the total number of simulated events and the number left after all cuts, these tables should give a good picture of the importance of the various cuts.

It is somewhat surprising that the demand that each of the two jets should contain at least one charged particle is important for the rejection of W-pairs.

Simulations with $\sqrt{s} = 161$ GeV, $\int L\,dt = 10pb^{-1}$						
Channel	MC events	$\int Ldt$ (pb^{-1})	After cuts	Fraction (%)	σ (pb)	# events
Background						
ff	48002	210	1	0.0021	228	0.047 ± 0.47
W^+W^-	51312	15091	347	0.68	3.4	0.23 ± 0.1
$We\nu$	1997	3767	20	1.0	0.53	0.053 ± 0.012
$\gamma\gamma \rightarrow$had(VDM)	5291	0.79	0	0	6700	0
$\gamma\gamma \rightarrow$had(VDM)	172276	24	0	0	7200	0
$\gamma\gamma \rightarrow$had(VDM)	71113	10	0	0	6900	0
$\gamma\gamma \rightarrow$had(QPM)	9537	12	0	0	820	0
$\gamma\gamma \rightarrow$had(QPM)	47796	50	0	0	960	0
$\gamma\gamma \rightarrow$had(QCD)	5807	2.9	0	0	2000	0
$\gamma\gamma \rightarrow$had(QCD)	53065	28	0	0	1900	0
$\gamma\gamma \rightarrow \tau^+\tau^-$	10854	27	0	0	396	0
$\gamma\gamma \rightarrow \mu^+\mu^-$	51223	26	0	0	1937	0
Total background						0.33 ± 0.11
Signal						
$M_H = 50$	1000	1754	257	26	0.57	1.5 ± 0.1
$M_H = 60$	1000	2857	304	30	0.35	1.1 ± 0.1
$M_H = 70$	1000	7142	293	29	0.14	0.41 ± 0.02

Table 6: Results from simulations with $\sqrt{s} = 161\ GeV$. The last column is the expected number of events corresponding to $10pb^{-1}$.

Simulations with $\sqrt{s} = 136$ GeV, $\int L\,dt = 2.9pb^{-1}$						
Channel	MC events	$\int Ldt$ (pb^{-1})	After cuts	Fraction (%)	σ (pb)	# events
Background						
ff	27582	69	2	0.0073	401	0.087 ± 0.061
W^+W^-	60	120	0	0	0.5	0
Z^0Z^0	60	133	2	3.3	0.45	0.045 ± 0.032
$We\nu$	60	666	1	1.7	0.09	0.0045 ± 0.0045
$Z^0e^+e^-$	120	20	0	0	6.0	0
$\gamma\gamma \rightarrow$had (QPM)	5694	7.2	0	0	790	0
$\gamma\gamma \rightarrow$had (VDM)	8217	1.3	0	0	6100	0
$\gamma\gamma \rightarrow$had (QCD)	6183	4.2	0	0	1480	0
$\gamma\gamma \rightarrow \tau^+\tau-$	1656	79	0	0	21	0
$\gamma\gamma \rightarrow \mu^+\mu^-$	11432	5.4	0	0	2109	0
$\gamma\gamma \rightarrow e^+e^-$	2163	5.4	0	0	401	0
Total background						0.14 ± 0.07
Signal						
$M_H = 50$	998	1720	345	35	0.58	0.60 ± 0.026

Table 7: Results from simulations with $\sqrt{s} = 136\ GeV$. The last column is the expected number of events corresponding to $2.9pb^{-1}$.

Simulations with $\sqrt{s} = 130$ GeV, $\int L\,dt = 3.0pb^{-1}$						
Channel	MC events	$\int Ldt$ (pb^{-1})	After cuts	Fraction (%)	σ (pb)	# events
Background						
ff	28361	61	4	0.014	463	0.20 ± 0.1
W^+W^-	60	150	1	1.7	0.4	0.020 ± 0.020
Z^0Z^0	60	133	1	1.7	0.45	0.022 ± 0.022
$We\nu$	60	666	1	1.7	0.09	0.0045 ± 0.0045
$Z^0e^+e^-$	120	20	0	0	6.0	0
Total background						0.25 ± 0.10
Signal						
$M_H = 50$	998	1720	345	35	0.58	0.6 ± 0.03

Table 8: Results from simulations with $\sqrt{s} = 130\ GeV$. The last column is the expected number of events corresponding to $3.0pb^{-1}$.

The final number of W-pairs is 188 out of 27933, and if this cut had not been included it would have been 36 more.

The cut in $\cos\theta/E_{\theta<30^\circ}$ is very important in the W-pair channel. As mentioned earlier the WW events with tau decays are very similar to the Higgs events. The only difference is in the polar angle distribution, and this cut exploits this fact.

As expected the cut in acoplanarity angle is crucial for rejecting $f\bar{f}$ events, but it also plays a substantial role in the rejection of the other background channels, especially the two-photon channels.

The upper limit on charged energy is absolutely necessary in order to avoid a large W-pair background. Without this there would be over three times as many W-pairs slipping through. Also for the Z-pairs it is important as it halves this background, but as the cross section is very small it would not have been necessary to have the cut this tight if there were no W-pairs.

The crucial cut for removing two-photon events is the cut in transverse momenta. Especially in the part of the hadronic channel that is simulated using the Vector Dominance Model it turns out to be of great importance.

It is interesting to see that the cuts in $\cos\theta/E_{\theta<30^\circ}$ and charged energy reject more signal events if the Higgs masses are high than with low masses while the opposite is true for the cuts in ϕ and p_t/E_{cha}.

The reason that more events are rejected by the cut in $\cos\theta$ with high masses can be understood when considering the $\sin^2\theta$ dependence of the differential cross section. Higgs particles at rest decay isotropically. When boosted the decay particles are also boosted, and they will tend to be moving in the Higgs particles direction and thereby mainly have large thrust angles.

The same argument can be used to explain the mass dependence of the effect of the cut in acoplanarity angle for signal events: The more the decay particles move in the Higgs particles direction the smaller the acoplanarity angles.

8.2 Exclusion and Discovery Limits

When estimates of background and signal efficiencies are ready, relevant questions are: With a certain luminosity, what is the highest Higgs mass that can be excluded? Or, how high can the mass be if a discovery is to be made? Discovery and exclusion are defined in appendix B.

Before answering these questions one has to decide the type of result one should use in these calculations. In [35] a *typical* result has been chosen. When talking about exclusion it means a result equal to the expected background, for discovery it is a result equal to the expected background and signal.

	ff	W^+W^-	$We\nu$	$Z^0e^+e^-$	Z^0Z^0
Events simulated	37827	27933	1000	3220	8651
After all cuts	3	188	7	1	51
$N_{cha,1,2} \geq 1$	6	36	6	1	4
$N_{charged} < 7$	1	8	18	0	47
$\cos\theta < 0.85$ $E_{\theta<30^\circ} < 7\%\ of\ \sqrt{s}$	1	36	2	1	7
$\phi < 20^\circ$	284	56	2	5	31
$p_t > 8.5\%\ of\ \sqrt{s}$ $E_{cha} > 4\%\ of\ \sqrt{s}$	2	2	4	0	5
$E_{cha} < \frac{\sqrt{s}}{4}$	0	448	3	2	79
E_{tot} <45% of $\sqrt{s}$	0	4	0	0	1

Table 9: Numbers of events removed by the individual cuts after all the other cuts have been applied at $\sqrt{s} = 192$ GeV.

	$\gamma\gamma \rightarrow$hadrons			$\gamma\gamma \rightarrow$lepton pairs	
	QPM	VDM	QCD	$\tau^+\tau^-$	$\mu^+\mu^-$
Events simulated	47796	172276	53065	10854	51223
After all cuts	0	0	0	0	0
$N_{cha,1,2} \geq 1$	0	0	0	0	0
$N_{charged} < 7$	0	0	0	0	0
$\cos\theta < 0.85$ $E_{\theta<30^\circ} < 7\%\ of\ \sqrt{s}$	0	2	0	0	2
$\phi < 20^\circ$	10	60	0	2	38
$p_t > 8.5\%\ of\ \sqrt{s}$ $E_{cha} > 4\%\ of\ \sqrt{s}$	17	72	6	20	42
$E_{cha} < \frac{\sqrt{s}}{4}$	0	0	0	0	0
E_{tot} <45% of $\sqrt{s}$	0	0	0	0	0

Table 10: Numbers of two-photon events removed by the individual cuts after all the other cuts have been applied at $\sqrt{s} = 161$ GeV.

	Signal				
	$M_H = 50$	$M_H = 60$	$M_H = 70$	$M_H = 80$	$M_H = 90$
Events simulated	1000	1000	1000	1000	1000
After all cuts	270	286	299	301	301
$N_{cha,1,2} \geq 1$	21	23	11	23	11
$N_{charged} < 7$	0	0	1	0	0
$\cos\theta < 0.85$ $E_{\theta<30^\circ} < 7\% \; of \; \sqrt{s}$	16	5	35	35	46
$\phi < 20^\circ$	96	94	78	55	61
$p_t > 8.5\% \; of \; \sqrt{s}$ $E_{cha} > 4\% \; of \; \sqrt{s}$	60	53	51	40	28
$E_{cha} < \frac{\sqrt{s}}{4}$	74	96	87	117	119
E_{tot} <45% of $\sqrt{s}$	5	3	1	3	3

Table 11: Numbers of signal events removed by the individual cuts after all the other cuts have been applied at $\sqrt{s} = 161$ GeV.

Table 12 gives the corresponding mass limits for discovery and exclusion with a given luminosity. The estimates of the backgrounds have been used without taking into account the uncertainties. The definitions of exclusion and discovery only consider exact expectation values.

If the result is equal to the expected background, masses up to M_{Excl} can be excluded. If Higgs bosons exist with a mass lower than M_{Disc} and the result is greater or equal to the sum of the expected background and the signal corresponding to the mass of the existing Higgs boson, then a discovery can be announced.

Only center of mass energies of 175 and 192 GeV are considered. With $\sqrt{s} = 161$ GeV the expected backgrounds are small and the term *typical* result is not well defined as only integer numbers can be used in the definition of exclusion. For example, with $\int Ldt = 40pb^{-1}$ the expected background is 1.32. What is the *typical* result?

The most probable result is 1. With that result the upper limit on the signal is 4.0 which corresponds to $M_H = 61$ GeV. In other words, with $\sqrt{s} = 161$ GeV and $\int Ldt = 40pb^{-1}$ masses up to 61 GeV can most likely be excluded if there is no signal. Compared to the numbers for 175 and 192 GeV, this is a much better result.

With $\int Ldt = 300pb^{-1}$ at 161 GeV and using the typical result for calculations, discovery can be made with masses up to 67 GeV. Masses up to 72 GeV can be excluded.

	175		**192**	
$\int Ldt$	M_{Excl}	M_{Disc}	M_{Excl}	M_{Disc}
40	43	-	47	-
80	60	-	60	-
120	67	32	65	42
160	71	40	68	47
200	74	48	70	52
240	76	54	72	56
280	76	57	73	58

Table 12: Mass limits corresponding to the integrated luminosities.

As this thesis is written, 10 pb^{-1} has been collected at 161 GeV and upgrading of the accelerator to higher energies has started. With this luminosity the expected background is 0.33, and if the result is zero, this excludes masses up to 26 GeV, not very interesting as masses up to 45.4 GeV already are excluded[5].

8.3 Conclusions from Simulations

During the LEP200 running (1996-98, possibly 99) an accumulated luminosity of more than 300 pb^{-1} is assumed to be collected. If most of the data have a center of mass energy equal to 192 GeV, as planned, Higgs masses up to at least 76 GeV can be excluded. Discovery cannot be done with masses higher than 57 GeV.

The best energy to search for charged Higgs bosons is around W-pair threshold or somewhat below. The W-pair background will be small and exclusion and discovery require much less luminosity.

9 Analysis of the 95-P3 data

In November 1995 LEP was, as the first e^+e^- collider, able to obtain a center of mass energy higher than the Z^0 mass and this meant possibilities of discovering "new" physics. During a period of a few weeks, DELPHI accumulated a total integrated luminosity of $5.9pb^{-1}$, 2.9 at 136 GeV, 3.0 at 130 GeV and 0.03 at 140 GeV. Unless the cross sections of the possible "new" processes are rather large, this is too little for exclusion or discovery. Anyhow, one can never know for sure what the cross section of a charged scalar is, so a search should be done. This was also a good opportunity for testing the analysis, and the quality cuts in impact parameters could be investigated.

9.1 Tuning Quality Cuts

As there were no available simulations of spurious events, beam wall, beam gas events, cosmics etc., there was no obvious way of eliminating them from the data. The method used in this analysis is to assume that all the other backgrounds are included in the simulations and then call the difference between data and simulations for spurious events. The quality cuts were then tightened until there was a good agreement between data and simulations. In all the figures in this section a preselected sample is used, consisting of two jet events with at least one charged particle in each jet.

In figure 20 the distribution in $\cos\theta$ is plotted for P3 data and the total simulated backgrounds with various limits on $b_{r-\phi}$ and b_z. The backgrounds included are $f\bar{f}$, W^+W^-, Z^0Z^0, $We\nu$, $Z^0e^+e^-$, Bhabha scattering and all the two-photon processes.

As there were no available simulations of two-photon processes at 130 GeV, the results from 136 GeV were also used for 130 GeV. The Bhabha contribution is put together from what is called "Bhabha Barrel", Bhabhas with θ greater than 37°, and "Bhabha Forward" which is produced with a generator optimized for the forward direction. All the events from "Bhabha Barrel" are used while only events with thrust angle greater than 37° are used in "Bhabha Forward". The Bhabha events in the $f\bar{f}$ samples are not included as they are already included.

As can be seen it is very important that the setting of the upper limits of $b_{r-\phi}$ and b_z is done properly. There is a large excess of data in the two upper plots were the limits are 6 and 18 cm and 4 and 12 cm. In the two lower plots where the limits are 2 and 6 cm and 1.5 and 4.5 cm the agreement is quite good. As tighter cuts give less signal efficiency the cuts of 2 and 6 cm are used. The preselection of P3 events satisfying these cuts contains 2950

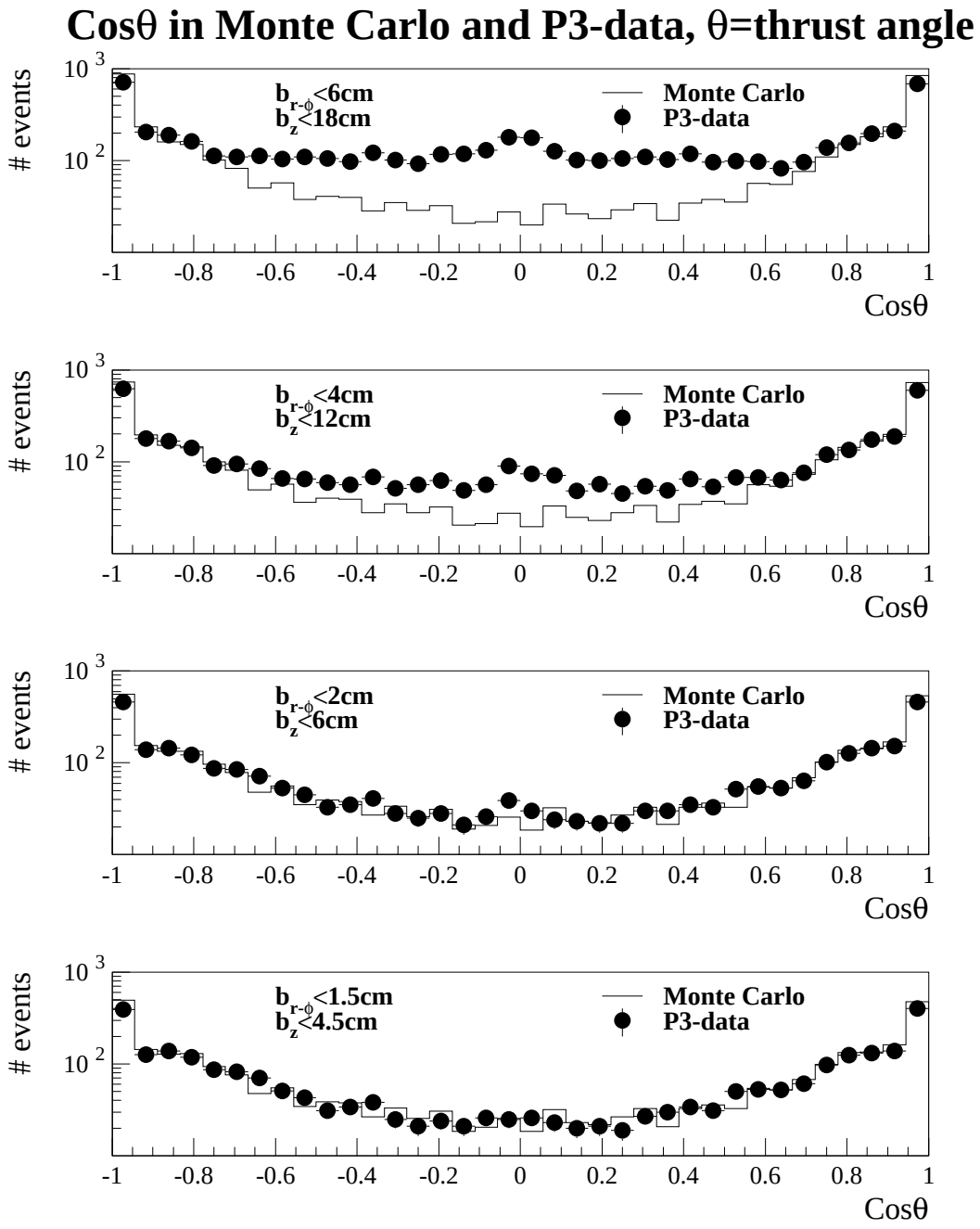

Figure 20: Plots of the $\cos\theta$ distribution in Monte Carlo and data. The upper limits on $b_{r-\phi}$ and b_z are decreased from 6 and 18 cm in the upper plot to 1.5 and 4.5 cm in the lower plot. Only events with two jets and at least one charged particle in each jet are included.

events. According to simulations it should have been 3099.

If one in addition requires that $|\cos\theta| < 0.85$ then the number of P3 events is 1550, and the number of simulated events is 1485. In order to understand of what kind these excess events are, the same comparison is done in the distribution of charged energy divided by the center of mass energy. See figure 21.

The agreement is again quite good except for the first bin where there are less simulated events than there are data events. There are also too many simulated events in the high energy region between 0.9 and 1.0.

It is not clear what the origin of these discrepancies is. In the low energy region it could be the uncertainties due to the small integrated luminosities of the two-photon simulations. The estimated cross sections can be too small or the fraction of events passing the cuts can be too small.

In the high energy region the explanation most probably is in the Bhabha simulations as this background is the dominant one. It could be that the reconstruction in the simulations are too optimistic, i.e. the events are better reconstructed than they should be, or again that the cross section given with the Monte Carlo DST's are wrong.

If the cuts in charged energy are applied, $4\%\ of\ \sqrt{s} < E_{cha} < \frac{3}{8}\sqrt{s}$, the number of P3 and simulated events are respectively 664 and 623. In figure 22 the distribution in acoplanarity angle is plotted. The agreement is not perfect, but one should remember that the axis is logarithmic, i.e. the number of events with large acoplanarity angles is small.

In figure 23 the distribution in impact parameters for signal events are shown. It is clear that the cuts in impact parameters are not removing much signal. In other words there is no problem associated with combining high signal efficiency and rejection of spurious events.

Even though the cuts in impact parameters make the distributions in data and simulations quite similar one should try to make at least a crude estimate of the background consisting of spurious events. As the final result in the P3 data is zero and the distributions in data and simulations are in reasonable agreement it is not very relevant for this analysis, but as a preparation for the analysis of the LEP2 data it is important. The final result of zero P3 events indicates that the background from spurious events is close to zero, but this could be by chance only. What is needed is a sample of spurious events that is larger than the sample included in the preselection so that the uncertainty can be decreased.

Spurious events have not been simulated so one can not just apply the cuts and then see what fraction of the spurious events that is left. However, if one could select a part of the P3 data containing only spurious events this could be used as an independent sample. The obvious way to do this

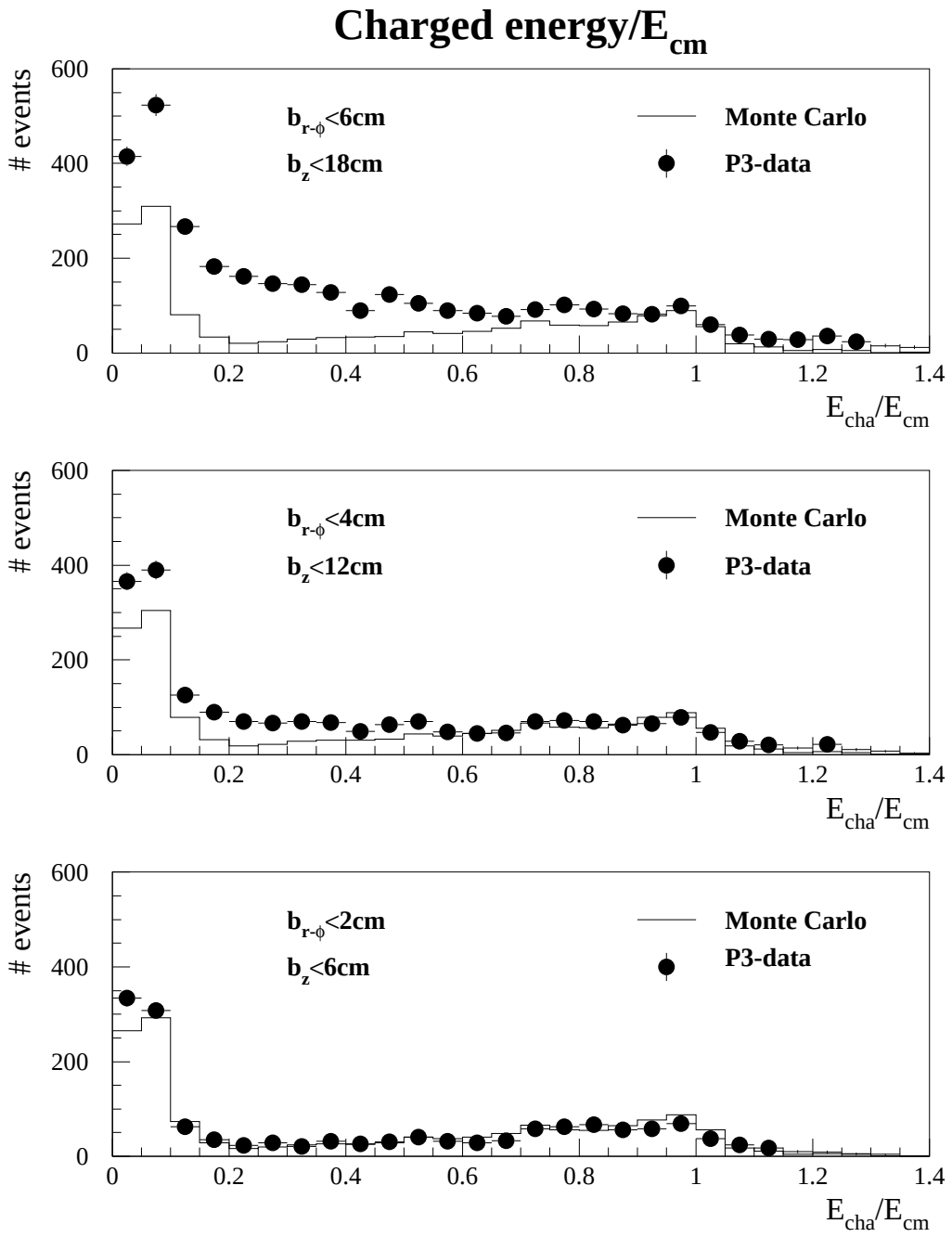

Figure 21: Plots of charged energy divided by $\sqrt{s}$ in Monte Carlo and data. The upper limits on $b_{r-\phi}$ and b_z are decreased from 6 and 18 cm in the upper plot to 2 and 6 cm in the lower plot. Only events with two jets and at least one charged particle in each jet are included, and $|\cos\theta| < 0.85$.

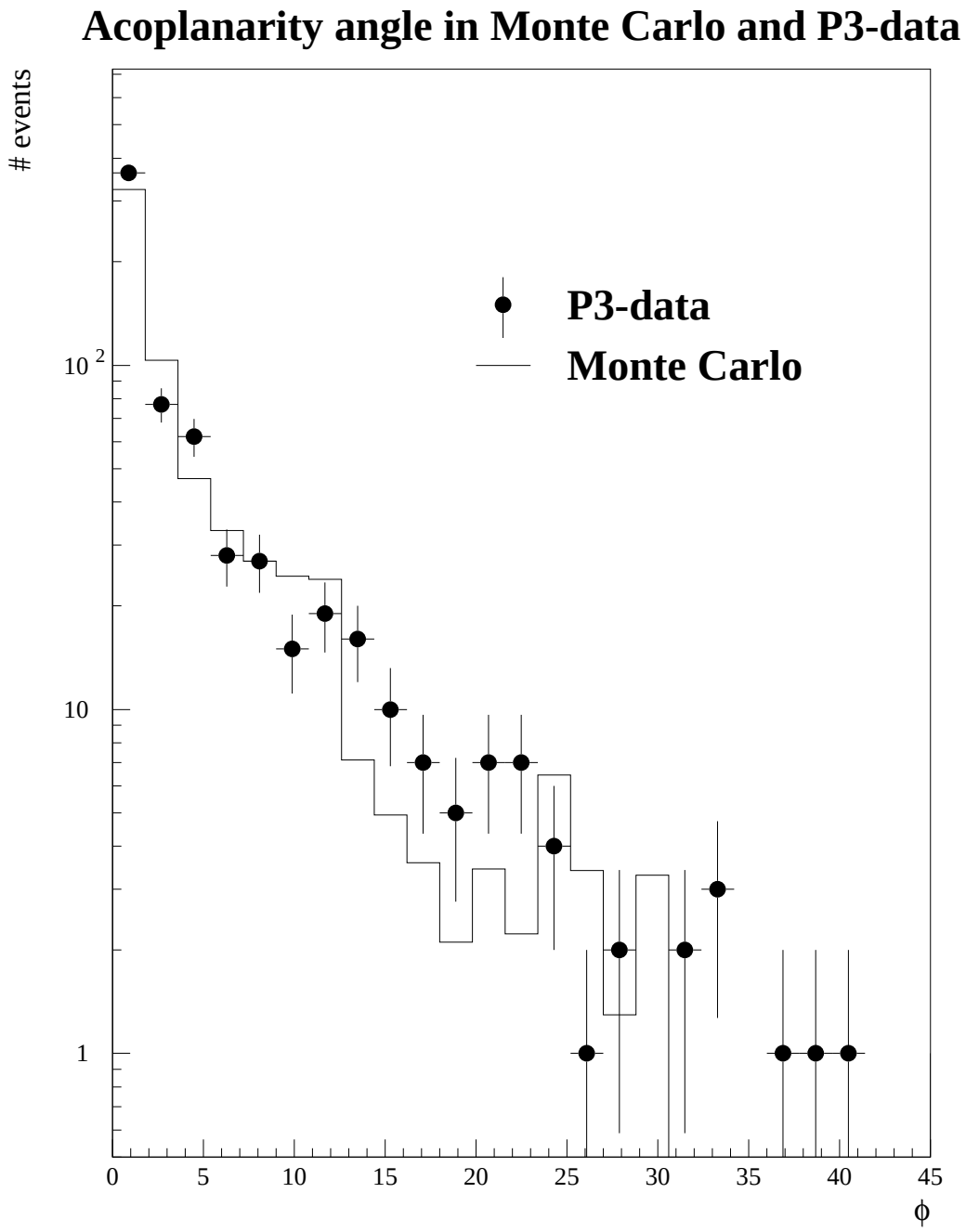

Figure 22: Plots of the acoplanarity angle in Monte Carlo and data. # jets=2, at least one charged particle in each jet, $|\cos\theta| < 0.85$ and $4\%\ of\ \sqrt{s} < E_{cha} < \frac{3}{8}\sqrt{s}$.

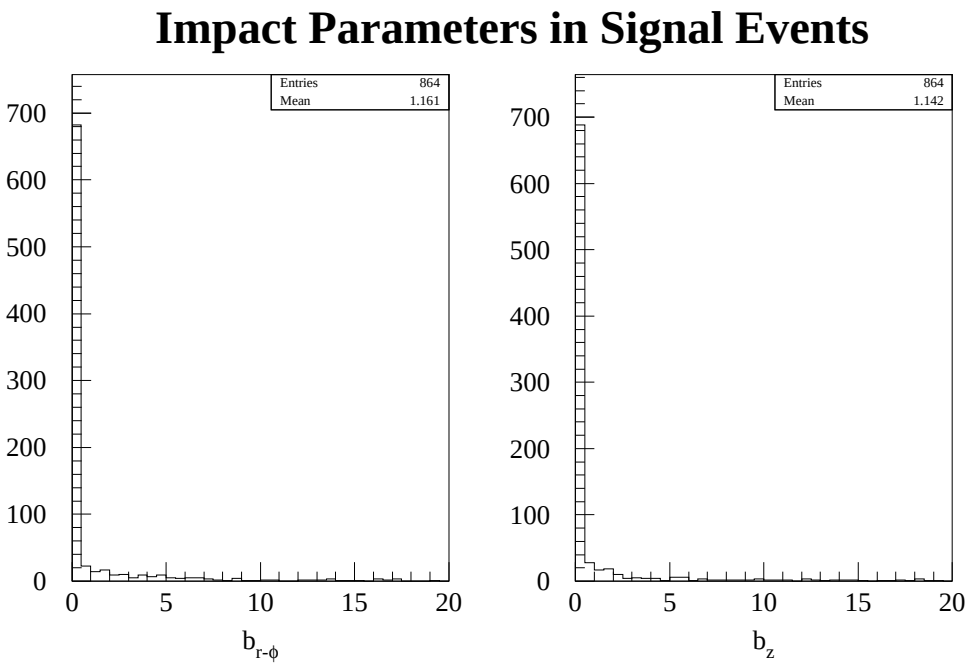

Figure 23: Plots showing the distribution in impact parameters, $b_{r-\phi}$ and b_z. For each event only the highest values found among the charged particles are used as these are the values in which the cuts are made. Only events with at least two charged particles are considered. The center of mass energy is 136 GeV.

is to exploit the characteristics of the wanted events, that is large impact parameters.

The largest impact parameter in events going in the forward direction tend to be higher than in other events. Hence, before selecting spurious events by demanding large impact parameters, events with $|\cos\theta| > 0.85$ are removed so that the number of events with large impact parameters that *are* included in the simulations is reduced. Also, only events with two jets and at least one charged particle in each jet are considered.

In figure 24 the distributions in impact parameters are compared for P3 data and simulated events. The simulated events are scaled to the integrated luminosity of the P3 data, 5.9 pb^{-1}. In the P3 distribution in b_z there is an odd peak at $b_z \approx 172$ cm. It turns out that the events constituting this peak all have an acoplanarity angle equal to approximately 180 degrees and the angle between the jets is 60.7 degrees. These events cannot be ordinary events, and therefore only events with $b_z < 150$ cm are considered. If the remaining P3 events with $b_{r-\phi} > 10$ cm and $b_z > 20$ cm are selected one can see that only a very small fraction are events included in the simulations. The number of events in this sample is 15075. When all the cuts are applied 10 of these events slip through.

As figure 25 shows these events are not located in one particular area of impact parameter space. This indicates that the other variables are not *strongly* correlated to the impact parameters.

The number of P3 events with $b_{r-\phi} < 2$ cm and $b_z < 6$ cm is 1550 while the number predicted by simulations is 1488. The difference is 62. In order to make a conservative estimation of the background from spurious events one can say that the selected sample of P3 events contains 150 spurious events. This corresponds to the difference of 62 plus 2σ where σ is the uncertainty in the difference. If one assumes that the same fraction of these spurious events slip through as for the spurious events with large impact parameters, this will give a background of 0.1 events.

It is of course quite unlikely that all the variables in which there is a cut are totally independent of the impact parameters. In other words, the fraction of spurious events slipping through with low impact parameters is probably not the same as with large impact parameters. However, using 150 as the number of spurious events with low impact parameters is rather conservative, so the background from spurious events should not be a problem when the LEP200 data are analyzed.

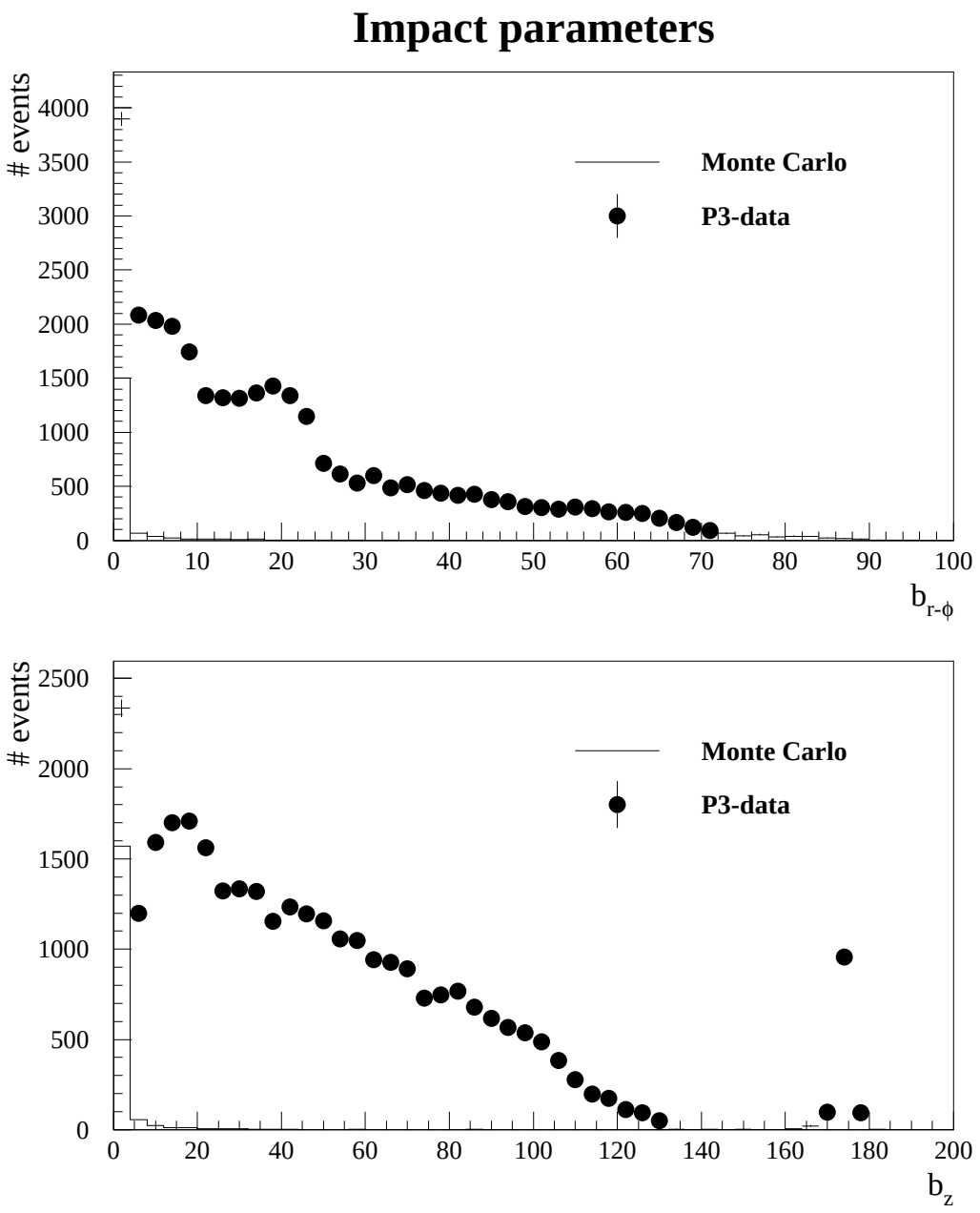

Figure 24: Plots showing the distributions in impact parameters, $b_{r-\phi}$ and b_z. For each event only the highest values found among the charged particles are used as these are the values in which the cuts are made. Events used have two jets, at least one charged particle in each jet, $|\cos\theta| < 0.85$, and less than seven charged particles.

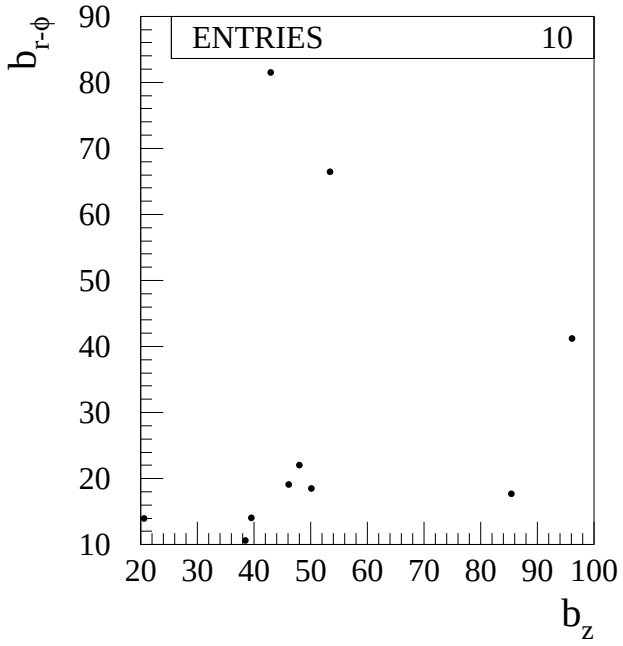

Figure 25: Plot showing the impact parameters of the 10 events with large impact parameters which slip through all the cuts.

9.2 Results

Table 13 gives the numbers of events remaining after each cut. The Monte Carlo results are divided into fermion-antifermions, Bhabhas, two-photon events and other events (W and Z pairs, $We\nu$ and $Z^0e^+e^{-1}$).

When all the cuts are applied there are zero P3 events left. The expected number from simulations is 0.39 ± 0.12. Using 0.39 as the expectation value of the background Higgs masses up to 30 GeV are excluded with a confidence limit of 95%. With 90% confidence masses up to 38 GeV are excluded.

	P3	**Simulations**				
		ff	Bhabha	$\gamma\gamma$	Other	Total
Preselection	2950	277	902	1920	4	3103
$\lvert\cos\theta\rvert < 0.85$	1550	253	581	651	3	1488
$4\%\ of\ \sqrt{s} < E_{cha} < \frac{3}{8}\sqrt{s}$	664	68	17	538	2	625
$p_t > 8.5\%\ of\ \sqrt{s}$	184	67	17	68	0	152
$\phi > 20^\circ$	1	1.0	0	0	0.1	1.1
All Cuts	0	0.28	0	0	0.11	0.39

Table 13: The row marked 'Preselection' gives the number of events satisfying the preselection criteria. In the next row the cut in $\cos\theta$ is applied, then the cuts in charged energy are added and so on. In the bottom row all the cuts are included.

10 Conclusions

So far we have no experimental information about the Higgs sector. We do not even know if Higgs bosons exist. The main reason for this is that the Higgs bosons are heavy and they couple to mass and thereby only weakly to the fermions ordinary matter is made of. The upgrading of the LEP accelerator means new possibilities for discovery. An analysis has been designed to find the charged Higgs boson. The Standard Model does not contain charged Higgs bosons, but if it is extended with an extra Higgs doublet it does. There are no experimental or theoretical results indicating the number of Higgs doublets.

As this is written runs at 130, 136 and 161 GeV are completed. The 95-P3 data (130 and 136 GeV) have been analyzed. Comparisons between data and simulations have been done in some of the variables used in the analysis. With proper settings of the cuts in impact parameters there is a good agreement. It is crucial that the upper bounds on impact parameters are tight enough.

With all the cuts applied there are zero charged Higgs events in the 95-P3 data. This result does not improve the present mass limits on the charged Higgs mass as the statistics are low. However, the analysis of the P3-data has not been useless as these data have provided a possibility to set the limits on impact parameters.

175 GeV will be reached within 1996 and runs at 192 GeV are scheduled for 1997-1999. The potential for discovery and exclusion of a charged Higgs particle with $B(H^{\pm} \rightarrow \tau\nu_{\tau}) = 1$ has been explored. If a discovery is made at LEP200 the Minimal Supersymmetric Extension of the Standard Model is ruled out as a possible theory. The first order mass relation $M^2_{A^0} = M^2_{H^{\pm}} - M^2_W$ in this theory gives a lower bound on the mass equal to 83.5 GeV as the present mass limit on A is 22 GeV.

The process representing the major part of the background at these energies is the W-pair production. The best center of mass energy to look for charged Higgs bosons with $B(H^{\pm} \rightarrow \tau\nu_{\tau}) = 1$ is therefore around or somewhat below W-pair threshold as the cross section for W-pairs has a steep climb around threshold energies. Unfortunately only 10 pb^{-1} has been collected at 161 GeV.

If 300 pb^{-1} is collected at 192 GeV as planned, masses up to 76 GeV can be excluded, discovery can be made with masses up to 57 GeV. If we could have the same luminosity at 161 GeV the numbers are 72 and 67 GeV. In other words, higher masses can be excluded at 192 GeV than at 161 GeV, but the opposite is true for discovery. 192 GeV is for the pessimists, 161 GeV is for the optimists. In any case, LEP200 will give us more knowledge about the Higgs sector, either as improved exclusion limits or as discoveries.

A The Charged Higgs Cross Section

The differential cross section is given by

$$d\sigma = \frac{|\mathcal{M}|^2}{FN} dQ$$

[8] where dQ is the Lorentz invariant phase space factor (dLips), F is the flux and N is the density of target particles. A Higgs pair can be produced through an intermediate γ or Z^0 and the corresponding vertex factors are $-ie(P+P')^\mu$ and $\frac{-ig\cos 2\theta_w}{2\cos\theta_w}(P+P')^\mu$ where P and P' are the four momenta of the Higgs particles[13] ($\vec{P}$ is pointing towards the vertex while $\vec{P}$' is pointing away from the vertex.). The total Feynman amplitude can therefore be written as a sum.

$$\mathcal{M} = \mathcal{M}_\gamma + \mathcal{M}_{Z^0}$$

The differential cross section consists of three terms, the electromagnetic, the weak and the interference term originating from $|\mathcal{M}_\gamma|^2$, $|\mathcal{M}_{Z^0}|^2$ and $Re(2\mathcal{M}_\gamma \mathcal{M}_{Z^0})$.

A.1 The Electromagnetic Term

Using the Feynman rules[8] and some identities of the γ_μ matrices[2] one finds that

$$-i\mathcal{M}_\gamma = \bar{v}(p',s')ie\gamma^\mu u(p,s)\frac{ig_{\mu\nu}}{q^2}(-ie)(P+P')^\nu$$

and

$$i\mathcal{M}_\gamma^* = (P+P')^\alpha ie\frac{ig_{\alpha\beta}}{q^2}\bar{u}(p,s)(-ie)\gamma^\beta v(p',s').$$

When averaging over the possible spin configurations and using the completeness relations[3] and some trace theorems[4] one finds (in the center of mass system) that

$$\overline{|\mathcal{M}_\gamma|^2}$$
$$= \frac{1}{4}\sum_{s,s'}\frac{e^4}{q^4}\bar{v}(p',s')\gamma^\mu u(p,s)(P+P')_\mu(P+P')_\beta\bar{u}(p,s)\gamma^\beta v(p',s')$$

[2] $(\gamma^0)^2 = 1$, $\gamma^{\mu\dagger} = \gamma^0\gamma^\mu\gamma^0$

[3] $\sum_{s,s'} u(p,s)\bar{u}(p',s') = \not{p} + m$, $\sum_{s,s'} v(p,s)\bar{v}(p',s') = \not{p}' - m$

[4] The trace of an odd number of γ_μ's vanish.
$Tr(\not{a}\not{b}\not{c}\not{d}) = [(a\cdot b)(c\cdot d) - (a\cdot c)(b\cdot d) + (a\cdot d)(b\cdot c)]$
$Tr(\not{a}\not{b}) = 4a\cdot b$

$$
\begin{aligned}
&= \frac{1}{4}\sum_{s,s'}\sum_{a,b,c,d}\frac{e^4}{q^4}\bar{v}_a\gamma^\mu_{ab}u_b(P+P')_\mu(P+P')_\beta\bar{u}_c\gamma^\beta_{cd}v_d \\
&= \frac{1}{4}\sum_{s,s'}\sum_{a,b,c,d}\frac{e^4}{q^4}(u\bar{u})_{bc}\gamma^\beta_{cd}(v\bar{v})_{da}\gamma^\mu_{ab}(P+P')_\mu(P+P')_\beta \\
&= \frac{1}{4}\sum_{a,b,c,d}\frac{e^4}{q^4}(\not{p}+m)_{bc}(\not{P}+\not{P}')_{cd}(\not{p}'-m)_{da}(\not{P}+\not{P}')_{ab} \\
&= \frac{1}{4}\frac{e^4}{q^4}Tr\left[(\not{p}+m)(\not{P}+\not{P}')(\not{p}'-m)(\not{P}+\not{P}')\right] \\
&= \frac{1}{4}\frac{e^4}{q^4}\left\{Tr\left[\not{p}(\not{P}+\not{P}')\,\not{p}'(\not{P}+\not{P}')\right]-m^2Tr\left[(\not{P}+\not{P}')(\not{P}+\not{P}')\right]\right\} \\
&= \frac{e^4}{q^4}\left[2(p\cdot(P+P'))(p'\cdot(P+P'))-(p\cdot p')((P+P')\cdot(P+P'))\right. \\
&\qquad\qquad\left.-m^2(P+P')\cdot(P+P')\right] \\
&= \frac{e^4}{q^4}\left[2\left(\frac{s}{2}-2|\vec{p}||\vec{P}|\cos\theta\right)\left(\frac{s}{2}+2|\vec{p}||\vec{P}|\cos\theta\right)-\left(\frac{s}{4}+|\vec{p}|^2+m^2\right)\left(s-4|\vec{P}|^2\right)\right] \\
&= \frac{e^4}{q^4}\left[\frac{s^2}{2}-8|\vec{p}|^2|\vec{P}|^2\cos^2\theta-\frac{s}{2}\left(s-4|\vec{P}|^2\right)\right] \\
&= \frac{2e^4}{q^4}|\vec{P}|^2\left(s-4|\vec{p}|^2\cos^2\theta\right) \\
&\approx \frac{2e^4}{q^4}|\vec{P}|^2 s\sin^2\theta
\end{aligned}
$$

The flux is the relative velocity times the density of particles.

$$F = v_{rel}N$$

In the completeness relations a normalization corresponding to a particle density of $2E$ was assumed, and working in the mass center system one finds

$$F = 2\frac{|\vec{p}|}{E}2E = 2\frac{|\vec{p}|}{\frac{\sqrt{s}}{2}}2\frac{\sqrt{s}}{2} = 4|\vec{p}| \approx 2\sqrt{s}$$

dLips is given by

$$dQ = (2\pi)^4\,\delta^{(4)}(P+P'-p-p')\frac{d^3P}{(2\pi)^3\,2E_{H^+}}\frac{d^3P'}{(2\pi)^3\,2E_{H^-}}$$

Putting it all together

$$d^6\sigma = \frac{\overline{|\mathcal{M}_\gamma|^2}}{2s^2}\frac{1}{(2\pi)^2}\delta^{(4)}(P+P'-P-P')\frac{d^3P}{2E^2_{H^+}}\frac{d^3P'}{2E^2_{H^-}},$$

and after the integration of P' one gets

$$d^3\sigma = \left.\frac{\overline{|\mathcal{M}_\gamma|^2}}{2s^2}\right|_{\vec{P}+\vec{P}'=\vec{p}+\vec{p}'} \frac{1}{(2\pi)^2}\delta(E_f - s)\frac{d^3P}{4E_{H^+}E_{H^-}}$$

A change of variable in the δ-function gives

$$\delta(E_f - Ei) = \frac{E_f}{4|\vec{P}|}\delta(|\vec{P}| - \tilde{P})$$

where $\tilde{P}$ is the Higgs momentum that correspond to a Higgs energy equal to the energy of the electron/positron. The integration over $|\vec{P}|$ gives

$$\begin{aligned} d^2\sigma &= \frac{\overline{|\mathcal{M}_\gamma|^2}}{8s^{\frac{3}{2}}}\frac{1}{(2\pi)^2}\tilde{P}\ d\Omega \\ &= \frac{e^4}{4s^{\frac{5}{2}}}\frac{1}{(2\pi)^2}\tilde{P}^3 sin^2\theta\ d\Omega \\ &= \frac{e^4}{16\pi^2 s^{\frac{5}{2}}}\left(\frac{s}{4} - 4M_H^2\right)^{\frac{3}{2}}\sin^2\theta\ d\Omega \\ &= \frac{e^4}{128\pi^2 s}\left(1 - \frac{4M_H^2}{s}\right)^{\frac{3}{2}}\sin^2\theta\ d\Omega \end{aligned}$$

The total electromagnetic cross section is given by

$$\sigma = \frac{e^4}{48\pi s}\left(1 - \frac{4M_H}{s}\right)^{\frac{3}{2}}.$$

A.2 The Weak Term and the Interference Term

The weak part of the Feynman amplitude is given by

$$-i\mathcal{M}_Z = K\bar{v}\gamma^\mu\frac{1}{2}\left(c_V - c_A\gamma^5\right)u\frac{g_{\mu\nu} - q_\mu q_\nu/M_Z^2}{q^2 - M_Z^2}(P - P')^\nu$$

and

$$i\mathcal{M}_Z^* = K^*(P + P')^\alpha\frac{g_{\alpha\beta} - q_\alpha q_\beta/M_Z^2}{q^2 - M_Z^2}\bar{u}\frac{1}{2}(c_V + c_A\gamma^5)\gamma^\beta v$$

where

$$K = \frac{ig^2\cos 2\theta_w}{2\cos^2\theta_w}.$$

For leptons $c_V = 1/2 - 2\sin^2\theta_w$ and $c_A = 1/2$. Because $m_e \ll \sqrt{s}$ the electron mass can be ignored, and the Dirac equation reads

$$p'_\mu \bar{v}\gamma^\mu = 0$$

for the positron and

$$p_\mu \gamma^\mu u = 0$$

for the electron. That means that $q_\mu q_\nu$ can be deleted from the propagator because $q = p + p'$. Now let $c_R = c_V - c_A$ and $c_L = c_V + c_A$. We then find that

$$c_V - c_A\gamma^5 = c_R P_R + c_L P_L$$

and

$$c_V + c_A\gamma^5 = c_R P_L + c_L P_R$$

where $P_L = \frac{1}{2}(1 - \gamma^5)$ and $P_R = \frac{1}{2}(1 + \gamma^5)$ are the left- and right-hand projection operators. In the relativistic limit these operators are equal to the helicity operators[8]. The matrix part of $|\mathcal{M}_Z|^2$ is

$$\bar{v}\gamma^\mu(c_R P_R + c_L P_L)u\bar{u}(c_R P_L + c_L P_R)\gamma^\mu v.$$

When inserting spinors with the four helicity combinations one finds that only the two with opposite helicities give non-vanishing contributions,

$$\bar{v}_R\gamma^\mu u_L \bar{u}_L\gamma^\beta v_R c_L^2$$

and

$$\bar{v}_L\gamma^\mu u_R \bar{u}_R\gamma^\beta v_L c_R^2.$$

These expressions do not contain any γ^5's, and except for a constant they are equal to the corresponding electromagnetic expressions. The amplitudes of these particular reactions are proportional to the entries $d^1_{1,0} = -d^1_{-1,0} = \sin\theta$ of the rotation matrix, and when squared they are equal. That means that the factors c_L^2 and c_R^2 can be replaced with the average of the two, $c_V^2 + c_A^2$.

The trick now is to add two similar expressions with equal helicities (positive and negative) for the electron and positron. This can be done because they are equal to zero: $\bar{u}_R\gamma^\alpha v_R = \bar{u}_R P_L\gamma^\alpha P_L v_R = \bar{u}_R\gamma^\alpha P_R P_L v_R = 0$. It is now possible to average over all the helicity states and the rest of the calculation is done in the same way as for the electromagnetic cross section. The calculation of the interference term goes very much like the calculation of the weak term. The total cross section finally reads

$$\sigma = M_W^4 G_f^2 \frac{(1 - 4M_H/s)^{\frac{3}{2}}}{24\pi s} \left(\frac{\cos^2 2\theta_w}{\cos^4\theta_w} \frac{c_V^2 + c_A^2}{(1 - M_Z^2/s)^2} + 16\sin^4\theta_w + 8\tan^2\theta_w \cos 2\theta_w \frac{c_V}{(1 - M_Z^2/s)} \right)$$

where the Fermi coupling constant is related to g by $g^2 = \frac{8M_W^2 G_f}{\sqrt{2}}$.

B Discovery and Exclusion

When estimates of backgrounds and signal are ready, what will a certain hypothetical experimental result say about the existence of the charged Higgs bosons? It is impossible to say that it does not at all exist or that it exists for sure, but one can say that with a certain probability there is a signal or that the cross section must be lower than a certain limit. The definitions of exclusion and discovery agreed upon by all the LEP experiments are given below[35].

Discovery A result can be called a discovery if the probability of finding more than the observed number, n_0, with the estimated background μ_B in the absence of a signal is less than the probability of getting a result outside the 5σ limit in a Gaussian distribution, that is with a probability less than 5.7×10^{-7}.

Exclusion The expectation value of the signal, μ_S, is excluded down to the value N with confidence limit α where N is defined as follows: In a random repeat of the experiment, given that the contribution from the background, n_B, is less or equal to n_0 and the expectation value of the signal $\mu_S = N$, the probability of getting a result, n_1, higher than n_0 is equal to $1 - \alpha$. It is common practice to use $\alpha = 0.05$.

In detail, using Poisson probabilities, it is a discovery if

$$1 - e^{-\mu_B} \sum_{i=0}^{n_0} \frac{\mu_B^i}{i!} \leq 5.7 \times 10^{-7}.$$

The probability p of finding more than n_0 events given that $n_B \leq n_0$ with $\mu_S = N$ is

$$p = P(n_1 > n_0 \mid n_B \leq n_0) = 1 - P(n_1 \leq n_0 \mid n_B \leq n_0) = 1 - \frac{P(n_1 \leq n_0 \ \cap \ n_B \leq n_0)}{P(n_B \leq n_0)}.$$

But if $n_1 \leq n_0$ then $n_B \leq n_0$ and

$$p = 1 - \frac{P(n_1 \leq n_0)}{P(n_B \leq n_0)} = 1 - \frac{e^{-(\mu_B + N)} \sum_{i=0}^{n_0} \frac{(\mu_B + N)^i}{i!}}{e^{-\mu_B} \sum_{i=0}^{n_0} \frac{\mu_B^i}{i!}}.$$

N is varied until $p = 1 - \alpha$.

References

[1] H. F. Jones, *Groups, Representations and Physics*, Institute of Physics Publishing, ISBN 0-85274-029-8 (1990).

[2] P. Becher, M. Böhm and H. Joos, *Gauge Theories of Strong and Electroweak Interactions*, John Wiley & Sons, ISBN 0-471-10429-9.

[3] T. Cheng and L. Li, *Gauge Theory of Elementary Particle Physics*, Oxford University Press, ISBN 0-19-851956-7.

[4] *Review of Particle Properties*, Phys. Rev. **D54** (1996) 1.

[5] DELPHI Collaboration, Zeit. Phys. **C67** (1994) 183.

[6] L3 Collaboration, Phys. Let. **B294** (1992) 457.

[7] ALEPH Collaboration, Phys. Reports, **216** (1992) 253.

[8] F. Halzen and A. Martin, *Quarks & Leptons*, John Wiley & Sons, Inc., ISBN 0-471-81187-4 (1984)

[9] L. H. Ryder, *Quantum Field Theory*, Cambridge University Press, ISBN 0-521-23764-5 (1985).

[10] F. Mandl and G. Shaw, *Quantum Field Theory*, John Wiley & Sons, ISBN 0-471-94186-7.

[11] D.A. Ross and M. Veltman, Nucl. Phys. **B95** (1975) 135.

[12] S. Glashow and S. Weinberg, Phys. Rev. **D15** (1977) 1958.

[13] J. F. Gunion, H. Haber, G. Kane and S. Dawson, *The Higgs Hunters Guide*, Addison-Wesley, ISBN 0-201-50935-0 (1990)

[14] E. Eichten, I. Hinchliffe, K. D. Lane and C. Quigg, Phys. Rev. **D34** (1986) 1547.

[15] DELPHI Collaboration, Nucl. Instr. Meth. **A303** (1991) 233.

[16] DELPHI Collaboration, Nucl. Instr. Meth. **A378** (1996) 57.

[17] William R. Leo, *Techniques for Nuclear and Particle Physics Experiments*, Springer-Verlag, ISBN 3-540-57280-5 (1994).

[18] A. Andreazza et al., Nucl. Instr. Meth. **A367** (1995) 198.

[19] M. Šiket, DELPHI Collaboration note, *An Investigation of Properties and Behaviour of The Straw Detector, DELPHI*, DELPHI 95-156 TRACK 83.

[20] C. Brand et al., Nucl. Instr. Meth. **A367** (1995) 129.

[21] DELPHI Collaboration note, *Proposal for the DELPHI Surround Muon Chambers*, DELPHI 92-139 TRACK 71 (21. Oct 1991).

[22] A. Maio et al., *STIC, The New DELPHI Luminousity Monitor* contributed to the Elba Conference, 1993.

[23] A. C. Benvenuti et al., DELPHI Collaboration note, *The DELPHI Small Angle Tile Calorimeter*, DELPHI 94-157 CAL 120.

[24] T. Sjöstrand, Computer Physics Commun. **28** (1983) 229.

[25] S. Nova et al., DELPHI Collaboration note, *MONTE-CARLO Event Generator for Two Photon Physics*, DELPHI 90-35 PROG 152, 19 November 1990.

[26] DELPHI Collaboration note, DELPHI 89-67 PROG 142, 10 July 1989.

[27] DELPHI Collaboration note, DELPHI 94-161 PROG 210, 20 December 1994.

[28] DELPHI Collaboration note, DELPHI 89-44 PROG 137, 17 May 1989.

[29] DELPHI Collaboration note, DELPHI 92-118 PROG 189, 5 September 1994.

[30] G. K. Bhattacharyya and R. A. Johnson, *Statistical concepts and methods*, John Wiley & Sons, Inc., ISBN 0-471-03532-7 (1977)

[31] C. Parkes, DELPHI Collaboration note, DELPHI 96-37 PHYS 610, 26 March 1996.

[32] DELPHI Collaboration note, DELPHI 92-166 PHYS 250, 17 December 1992.

[33] T. Sjöstrand, Computer Physics Commun. **82** (1994) 74.

[34] E. Fahri, Phys. Rev. Lett. 39 (1977) 1587.

[35] Appendix, Interim report on the physics motivations for an energy upgrade of LEP2 by the Workshop on Physics at LEP2, CERN-TH/95-151, CERN-PPE/95-78.